CHALMERS
UNIVERSITY OF TECHNOLOGY

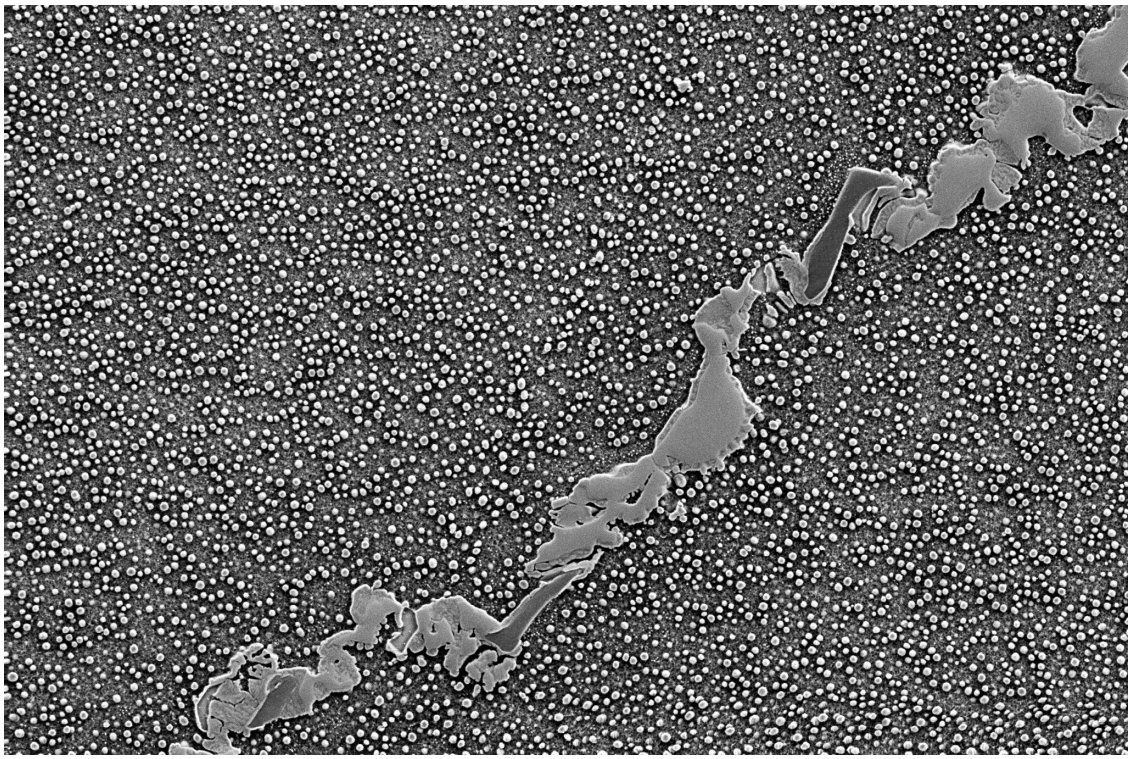

Heat Treatment Optimization for Nickel-based Cast Superalloy

In collaboration with GKN Aerospace

Master's thesis in Materials Engineering

David Ancona Orozco

DEPARTMENT OF INDUSTRIAL AND MATERIALS SCIENCE

CHALMERS UNIVERSITY OF TECHNOLOGY
Gothenburg, Sweden 2021
www.chalmers.se

Master's thesis 2021

Heat Treatment Optimization for Nickel-based Cast Superalloy

In collaboration with GKN Aerospace

DAVID ANCONA OROZCO

CHALMERS
UNIVERSITY OF TECHNOLOGY

Department of Industrial and Materials Science
Chalmers University of Technology
Gothenburg, Sweden 2021

Heat Treatment Optimization for Nickel-based Cast Superalloy
In collaboration with GKN Aerospace
DAVID ANCONA OROZCO

Supervisor: Géraldine Puyoo, GKN Aerospace
Examiner: Fang Liu, IMS

Master's Thesis 2021
Industrial and Materials Science
Chalmers University of Technology
SE-412 96 Gothenburg
Telephone +46 31 772 1000

Cover: SEM image of cast Haynes 282 microstructure.

Printed by Chalmers Reproservice
Gothenburg, Sweden 2021

Heat Treatment Optimization for Nickel-based Cast Superalloy
In collaboration with GKN Aerospace
DAVID ANCONA OROZCO
Department of Industrial and Materials Science
Chalmers University of Technology

Abstract

Nickel-based superalloys are broadly used in the aerospace industry for applications at elevated service temperatures. Haynes 282 is a recently developed, gamma-prime (γ') strengthened, nickel-based superalloy that can be manufactured in different ways, such as wrought methods, powder methods, and castings. An important difference between these methods is the lower mechanical performance found in the cast version of the alloy. A way to improve the mechanical properties of cast Haynes 282 is through a tailored heat treatment that considers the different properties of the material and the microstructural changes required.

The objective of this thesis work was to define alternative heat treatments to improve the ductility and strength of cast Haynes 282. These proposals were based on different studies found in literature, simulations, and microstructural analysis performed at GKN Aerospace. The heat treatments were tested and compared with reference values from the standard heat treatment recommended by Haynes International, and with a standard heat treatment developed by GKN. The tensile tests were carried out at room and elevated temperature, and their results, in combination with the microstructural analysis of the secondary phases performed in the different heat treated samples, showed an improvement in mechanical properties from a couple of heat treatment proposals. A proposed heat treatment, labeled HT10, showed a potential improvement of tensile strength, ductility and containment properties at an elevated temperature of 750 °C. Haynes standard heat treatment also showed improved properties between the two temperatures, when compared to the standard GKN heat treatment.

Keywords: Nickel superalloy, Haynes 282, heat treatment, mechanical properties, microstructure, ductility, containment, cast material, precipitation, gamma prime, carbides.

Acknowledgements

First of all, I would like to thank all the people that support me during this two-year journey in Sweden, with the ups and downs and all the challenges along the way. It has been a wonderful and rich experience in all the senses. I could not have done this without the support of my family, friends, in both Sweden and Mexico, and colleagues. Thank you all !

A big thank you to everyone that helped me, in different ways, during this thesis, at GKN and at Chalmers. Thanks a lot to my supervisors in this thesis, Fang at Chalmers, and Géraldine at GKN, who were there all along the thesis. I have learned a lot in these 6 months, and it has been thanks to you. To Fang, who supported me all the time during the project and helped with good advice in how to approach things. In GKN, a special thank you to Géraldine who guided me in this project, helped me a lot in all the different things done in the thesis, and also gave me a nice introduction into this industry!

I want to recognize and acknowledge all the people that in a certain way or the other supported me during my masters. From GKN, I would like to thank all the people in the department, Bengt, Prajina, Frank, Jesper, Peter; in the lab, Patrick, Johan, Niklas, Dennis, and everyone that spend some of their time into giving some orientation and share their experience with me. Thanks!

A big shout out to my friends at Chalmers, Fardan, Sachin, Arvid, and Christian; it has been a wonderful time getting to know you guys and also learning about all kinds of subjects. I also want to acknowledge Iu, Daniel, Pauline, Joaquin and Zuher; it has been great to meeting you all, and thanks for making a fun and great work environment at GKN.

Por último, quiero agradecer de nuevo a mi familia por todo el apoyo que me dieron todo este tiempo. Gracias a mis papás, hermana, amigos, y todos los que me apoyaron en algún momento. Siempre recordaré todo lo que hicieron para que esto fuera posible. Fue toda una aventura, pero al final una gran experiencia que me ha hecho crecer de varias formas, profesionalmente y como persona. Esto nunca pudo suceder sin todo su apoyo y amor. ¡Gracias!

David Ancona Orozco, Gothenburg, June 2021

Contents

List of Figures

List of Tables

1

Introduction

Nickel-based superalloys have been broadly used in the aerospace industry for different components in turbine engines due to their good performance at elevated temperatures. Along the years, one of the main objectives of the industry has been the increase in operation temperature of the aeroengines in order to increase their efficiency. Because of this increase in service temperature, new alloys have been developed to fulfill new requirements.

The increasing temperatures have demanded to increase even further the mechanical properties at elevated temperatures, such as the yield strength, ductility, containment (absorption of energy from impacts caused by detached components), and high temperature creep. Additionally, the materials must also present good properties on formability and weldability, which usually counteracts the desired mechanical properties. A way to measure the improvements in mechanical properties of the material, the containment factor (CF) has been used to describe the variation in them. This factor has been used in the industry to describe the containment properties in case of an engine failure [15].

One option that fulfills these requirements is the recent developed Haynes 282 alloy. Haynes 282 is a gamma-prime (γ') strengthened Nickel-based superalloy with good mechanical properties at elevated temperature and excellent formability, compared to other existing alloys, such as Waspaloy or R-41 alloy. Since the development of Haynes 282 alloy, different heat treatments have been studied in order to increase the mechanical properties at high temperatures. A limiting aspect of the results obtained is the lower ductility and strength for cast versions of the material, in comparison to wrought components.

The importance of improving the ductility, containment, and strength at both high and room temperatures for castings has defined the main purpose of this master thesis in which new heat treatment alternatives will be studied and selected to increase the desired properties.

2

Theory

The process in which a commercial aeroengines works consist in four main steps that take place in different parts of the engine. The process begins with air being suctioned by turbo-fans at the front side of the engine. The airflow is then directed to a compressor in the mid-section of the engine, in which it is compressed by rotors and stators, increasing the temperature of the system. The next step occurs in the combustion chamber, where the compressed air is mixed with fuel and ignited, to later use its combustion and expansion for thrust. The last section of the engine consists in turbines that use the expanded gases coming from the combustion chamber for rotation. The turbines rotation is then translated by a shaft to the front of the engine, resulting in the rotation of the front turbo-fans, allowing the process to continue. These process can be observed in Figure 2.1, in which the four main sections are shown.

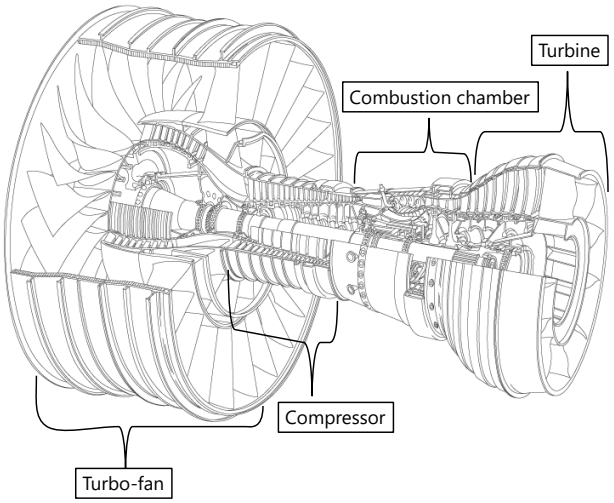

Figure 2.1: Sections of turbine engine. GKN Aerospace Webpage: *www.gknaerospace.com/en/our − solutions/engines/*

Something important to note is the increasing temperature that occurs from the beginning to the end of the process, resulting in a division of the engine depending on this temperature. Because of this, the engines are commonly divided in a cold section and a hot section, with different requirements, and hence materials, in each section.

Constant improvement and development in the design of turbine engines is one of the key elements of the aerospace industry, due to the effect it has on the performance of the whole craft. An important factor in the development of these engines is the

service temperature of the hot section in which it operates, since this section is the one that defines the efficiency of the engine [1]. The service temperature of this section is inversely proportional to the fuel consumption of the engine, resulting in a constant effort from the industry to increase that temperature. The action of increasing the service temperature in the turbine engine redefines the requirements each component must fulfill when operating, including the mechanical properties, corrosion resistance, and thermal stability.

In order to meet these requirements, different materials have been developed and applied in the industry, such as nickel-based superalloys. These alloys are characterized by their good performance at high temperatures and resistance to detrimental effects of working in those conditions. Also, they are known by the challenges their manufacturing processes present, in order to reach the final component design. A balance between the desired properties and the ability to manufacture the component is needed for these alloys, which leaves few room for the alloys to improve.

2.1 Nickel-based superalloys

Nickel-based superalloys refers to a group of alloys that stand out due to the high stability of their mechanical properties present at elevated temperatures, above 540 °C, in comparison to other type of materials such as Titanium-alloys. The reason of the good performance is due to a stable FCC matrix during heating and the low mismatch it has with its secondary phases. One way to classify nickel-based superalloys is by the type they are strengthened, which can be in two ways: gamma-double-prime (γ'') precipitation strengthened, or gamma-prime (γ') precipitation strengthened, plus a solid solution strengthening contribution which both have.[2, 1]

The γ''-strengthened superalloys are characterized by the precipitation of a γ'-phase Ni_3(Ti,Al) and the precipitation of a γ''-phase Ni_3(Nb), in which the latter is the principal strength contributor. Due to the stability temperature range of γ'', the operating temperatures these superalloys possess are limited to an upper limit of 650 °C approximately in which a detrimental δ phase forms. In these group, it is possible to find alloys such as IN-718 and IN-706, which are commonly used in the aerospace industry in certain components.

On the other hand, the γ'-strengthened superalloys present excellent mechanical properties resulting from a low lattice mismatch of ± 0-0.2 % between γ-matrix and γ', allowing their operation at higher temperatures, up to approximately 900 °C, depending on the alloy [3, 4] . In this group it is possible to find alloys such as Waspaloy, René-41, and Haynes 282, in which the latter has stood out in the aerospace industry due to a combination of good mechanical properties and formability.

In addition to the precipitation strengthening phases found, there is a second strengthening mechanism caused by solid solution strengthening. This mechanism consists in the presence of solute atoms in the lattice causing a mismatch with the matrix.

2.1.1 Haynes 282

Haynes 282 is a Nickel-based gamma-prime-strengthened superalloy developed by Haynes international [3]. Its chemical composition is characterized by the alloying of Al and Ti for precipitation strengthening, high content of Cr for corrosion resistance properties, high content of Mo for solution strengthening, among other elements to fine tune its properties [5, 6] . The main phases Haynes 282 present in both wrought and cast version are principally a γ-matrix, a Ti-rich and Al-rich γ' precipitant phase, Ti-rich and Mo-rich MC primary carbide phase, and Cr-rich $M_{23}C_6$ and Mo rich M_6C secondary carbide phases.

The temperature in which these phases are present can be observed in below, represented in a Scheill solidification simulation obtained using JMat Pro for a standard Haynes 282 composition. It is possible to see the solvus lines for the secondary phases mentioned above, in which $M_{23}C_6$ has a solvus temperature of 950 °C, 1150 °C for M_6C, and 1003 °C approximately for γ'. The ranges in which these phases are present will play a key role for the design of the manufacturing process the alloy will go through.

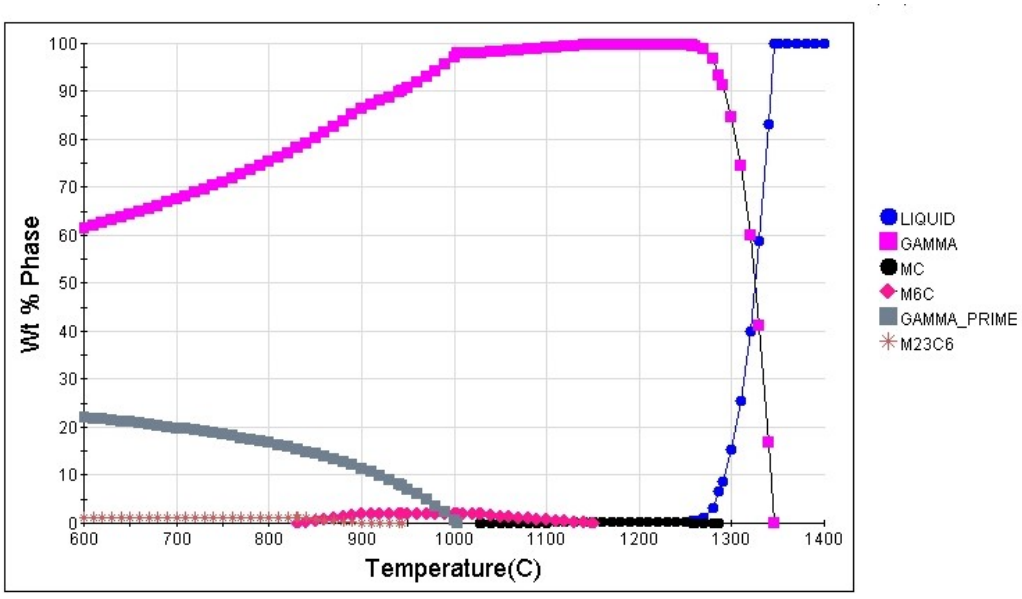

Figure 2.2: JMat Pro solidification simulation for Haynes 282

It is important to note that the presence, morphology, and volume fraction of these phases depends on the manufacturing process conditions and any heat treatment the alloy have gone through.

Haynes 282 received the attention of the aerospace industry due to the excellent thermal stability of its mechanical properties and good formability. In comparison with other similar superalloys available in the industry, Haynes 282 shows a higher creep strength than Haynes 263, Waspaloy, and René-41, while having better

formability and weldability than the last two. It also shows a lower thermal expansion, in addition to a positive increase in yield strength after thermal exposure, in comparison to the other above mentioned alloys [3].

There are different ways to process Haynes 282, including wrought or a cast products, each one with a characteristic microstructure and their respective mechanical properties depending on it. An important characteristic of Haynes 282 is that it can be processed as a wrought product and go through different thermo-mechanical processes, but also it can go through a casting process for the production of more complex and cost-effective products. As expected, there is a clear difference in the properties each version of Haynes present and in the following sections, these differences will be described in detail.

2.1.1.1 Wrought Haynes 282

The manufacturing process required to produce any wrought product consist in the heating and deformation of an ingot until the final shape of the product is achieved [1]. This process also apply to Haynes 282, resulting in a specific and unique microstructure, in comparison to its cast version.

Wrought Haynes 282 possess a microstructure defined by a equiaxed grains in the range of 20 μm to 100 μm. In certain conditions, depending on the process, e.g. forged or hot rolled, the grains may present a preferred orientation parallel to the deformation axis. After the wrought manufacturing process, the alloy is usually treated to obtain an initial condition in a mill-annealed state, through a heating process in the range of 1121-1149 °C during 30-60 minutes, usually air cooled to room temperature [3, 7, 8]. The grains present in a mill-annealed wrought Haynes 282 consist of an ordered FCC γ-matrix with dispersed primary MC carbides, in the inter-granular and intra-granular regions, formed since the solidification process.

In order to meet the mechanical requirements for an aeroengine application, the material has to go through a heat treatment to reach the precipitation-strengthened state. The recommended heat treatment by Haynes International consist in a solution-annealing step in the range of 1121-1149 °C, followed by a two-step treatment, first at 1010 °C for 2 hours and then at 788 °C for 8 hours [3]. After the recommended standard heat treatment, the resulting microstructure in wrought Haynes 282 consist of fine equiaxed grains with a fine dispersion of γ' precipitants, usually in spherical shape and size of 20 nm approximately [9].

The mechanical properties obtained from this heat treatment are a yield strength (YS) value in the range of 650-720 MPa approximately, an ultimate tensile strength (UTS) of 845-1100 MPa approximately, and an elongation in the range of 16-30 % [2, 5]. Finally, the hardness levels found in these products present a value of 310-370 HV approximately [7, 5]. The reason of the range the mechanical properties has been reported in literature for wrought Haynes 282 is the effect of the initial form and geometry the alloy has before the heat treatment is applied. All these properties can be modified by changing the parameters in the different heat treatment steps.

2.1.1.2 Cast Haynes 282

A cast product is formed by melting the metal and pouring it into a mold, in which the material solidifies and then taken out. There are different casting processes in which materials can go through, but for Haynes 282 and nickel-based superalloys, one of the most common way to cast them is through investment casting. This process consists on first producing a wax pattern resembling the final casting, which is dipped in a ceramic slurry to form a mold. The disposable pattern is then removed, leaving a hollow ceramic shell which is then filled with the alloy. After solidification, the ceramic mold is removed, leaving the component ready for post-process. [1]

The as-cast microstructure of Haynes 282 differs from its wrought version mainly due to the dendritic structure it presents. The phases present in this state is generally a γ-matrix, γ' formed during the solidification, primary Mo-rich and Ti-rich MC carbide, and in some cases there has been evidence of TiN primary nitrides, σ TCP phases, carbosulphides, and borides [10, 11]. An interesting point by *Matysiak et. Al*, is a difference in γ' size and morphology between dendrite and interdendrite regions of the as-cast Haynes 282, with a spherical morphology and size of 74 nm in dendritic regions and a cubic morphology and size of 113 nm in interdendritic regions [10]. The main cause of the difference in the phases found between each region is the micro-segregation of solute in the interdendritic region. This segregation comes from the solidification process and the high solute content found in the material. Micro-segregation not only result in different precipitation of γ', but also in a concentrated presence of primary carbide in the interdendritic region, due to segregation of C, Ti and Mo, which are carbide formers [10].

In addition to the micro-segregation and the dendritic structure found in the as-cast state of Haynes 282, cast products does not present a 100% density, with pores distributed along the cast. Because of this, material homogenization has become a required step in the processing of the material. In order to reach a full dense state, the cast goes through a Hot isostatic pressing (HIP) step, in order to homogenize and remove the porosity of the material. The process consists in taking the cast material through a period of elevated temperature and pressure during a period of time.

Generally, cast products after HIP and heat treatment have larger grains, 100-300 μm, compared to wrought products, 20-100 μm, leading to different mechanical properties . In comparison with wrought Haynes 282, casts show lower elongation and strength [11]. For creep strength at high temperature, cast nickel-based superalloys are expected to perform equal or better than wrought products, something confirmed in literature, in which cast Haynes 282 had a similar performance [1, 11].

One advantage cast version of any material has over wrought processes are the reduced cost it has in the industry, since near-net shape products can be produced with this method, including the possibility of complex internal features [1]. Because of this, tailored heat treatments for cast products have been studied in order to adjust the mechanical properties required.

2.2 Heat treatment for Haynes 282

The heat treatment of an alloy is a process in which the material goes through a sequence of steps at different temperatures during different periods of time for the purpose of improving its mechanical properties by modification of its microstructure. This sequence is usually tailored to the composition and state of the alloy, and the desired properties and microstructure.

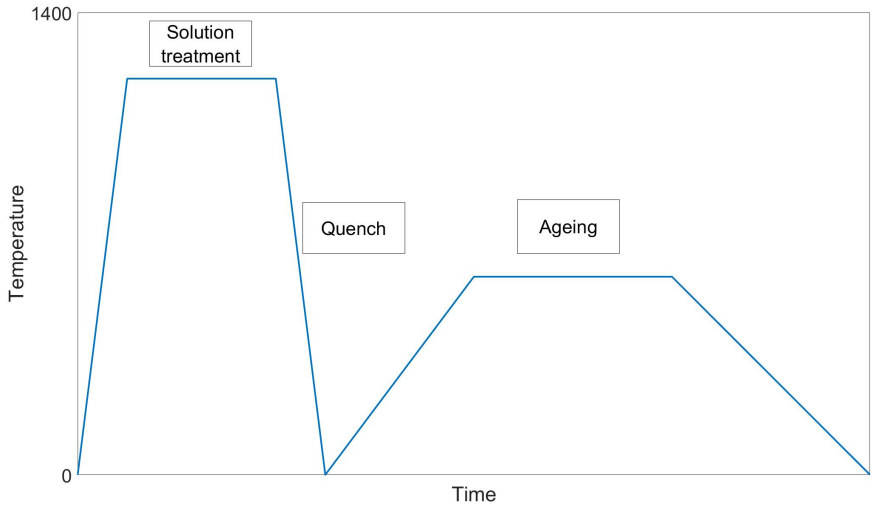

Figure 2.3: Common heat treatment for Nickel-based superalloys

Nickel-based superalloys generally receive a heat treatment based in three main stages, a solution heat treatment at a high temperature followed by a rapid cooling, and an ageing heat treatment at medium temperature in which precipitation of strengthening phases occurs [1]. This process can be observed in Figure 2.3, in which it is possible to see the different steps described previously, and the usual change in temperature and time.

The microstructure of the material will change in each of the heat treatment steps, and its characteristics after the whole sequence, e.g. phases distribution and size, will determine the mechanical properties that are present. The purpose of the solution heat treatment step is to dissolve the secondary phases found in the initial condition, due to their formation during the solidification process; these secondary phases can be secondary carbides $M_{23}C_6$ or even fine γ', The solution treatment is done at temperatures above the solvus temperature of the secondary phases. As mentioned, it is followed by a rapid cooling, usually quenched, which main purpose is to obtain a supersaturated solid solution that will allow the desired precipitation during the ageing step. Finally, the ageing step has as an objective the precipitation of secondary phases that will be in charge in strengthening the material, with an acceptable level of ductility. An important factor during the whole heat treatment are the cooling rates used between each step, since these affect the nucleation and

growth of the different phases that are present.

Something important to note is that it does not necessarily have to include just one ageing step, since it is common to combine different steps in order to lead the precipitants to an optimal combination of size and volume fraction, resulting in the desired final properties. In the case of Haynes 282, the recommended heat treatment consists on a solution treatment followed by a two-step ageing, which are usually called carbide stabilization step and precipitation step, respectively.

For Haynes 282, the standard and recommended heat treatment consists in a solution treatment step above the solvus temperature of the secondary phases at 1121-1149 °C approximately. In this step only primary MC carbides will be found in the microstructure, while secondary carbides and γ' precipitates will be dissolved. The next step is called a carbide stabilization step, done at 1010°C for two hours, to form secondary carbides at grain boundaries, while avoiding the formation of γ' precipitates. The third and last step has the objective to precipitate the strengthening secondary phases, through an ageing step of 788 °C for 8 hours [3]. The complete heat treatment scheme can be seen in Fig. 2.4.

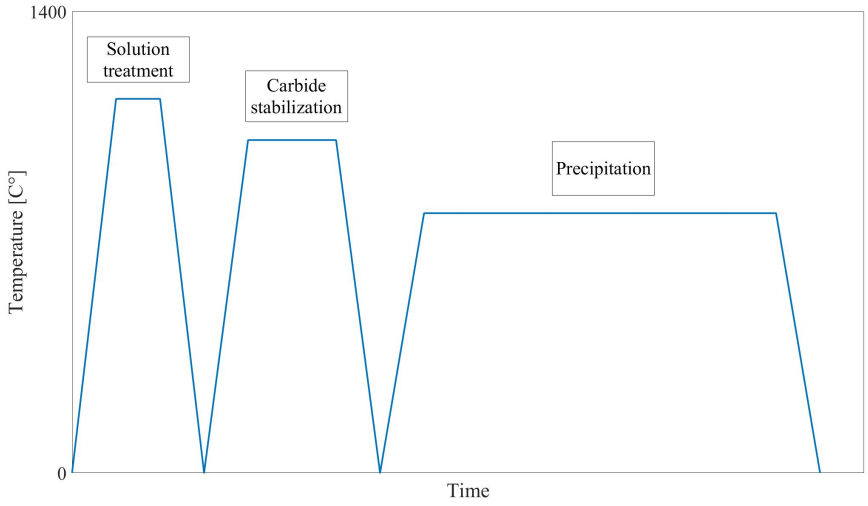

Figure 2.4: Recommended standard heat treatment by Haynes International

Based on the standard heat treatment recommended by Haynes International, several investigations have taken place to understand the effect of varying time and temperature along the process. The investigations have mostly been focused in the wrought version of Haynes 282, while the cast products have been studied, but not as frequent. These studies have been used as a reference to tailor the mechanical properties of the alloy as requested by GKN Aerospace. In the following sections, the specific changes due to the variation of parameters in each heat treatment step will be explained for the main secondary phases of the material.

2.2.1 Gamma prime evolution

In order to understand the changes that Haynes 282's mechanical properties go through during heat treatment, it is necessary to analyze the characteristics of its main strengthening phase, γ'.

The first important characteristic of γ' phase is its solvus temperature, which represents the temperature at which γ' starts to form while decreasing the temperature. Based in the Scheill simulation done for the standard composition of Haynes 282, Fig. 2.2, it is possible to see that the solvus temperature of γ' is found at 1003 °C. In addition to this, literature has stated that the temperature is 997 °C [12].Another solvus temperature for γ' has been reported by *Joseph*, based on experimental data, showing presence of γ' above 1010 °C, but a lack of it below 1024 °C [5].

By taking as a reference the solvus temperature of γ' at 997 °C, according to *Pike*, it is possible to understand why the standard heat treatment recommends a solutionizing step at 1010 °C for 2 hours. An important factor to consider is the experimental evidence showing that this temperature may not assure the complete dissolution of γ', specially in cases where coarse γ' already exists in the material.

Once the solution treatment step is over and most of γ' is dissolved,the precipitation stage of the heat treatment begins, and the shape, size and amount of the phase will depend on the time and temperature this step consist on. As mentioned before, the morphology of γ' can variate from cubic shape to spherical shape, and it is possible to find bi-modal γ' in the same microstructure [5, 10]. The same thing occurs with γ' size and volume fraction, since nucleation can occur in different steps, and its growth will variate the final size of the precipitants, resulting in a bi-modal γ'.

In order to characterize the change in volume fraction and size of γ', JMat Pro precipitation simulations were performed for standard composition of Haynes 282. The results of those simulations estimated the amount and size of γ' formed in each step of the heat treatment. As a starting point, the standard heat treatment was simulated and compared to observations done in literature. The data obtained presented a close match between the simulation and literature. The simulation results can be observed in section 4.

From the simulations, a general idea of how the main strengthening precipitate is obtained and how it is affected by the heat treatment modifications. This information served as a basis for the selection of alternative heat treatments for cast Haynes 282, which will be further explained in section 3.

2.2.2 Carbides evolution

In addition to the main γ' phase of Haynes 282, there are other important phases which contribute to both strength and, mostly, ductility of the material. These phases are the Cr-rich $M_{23}C_6$ and Mo-rich M_6C secondary carbide phases, which are formed from primary MC carbides found in the material before heat treatment.

$$MC + \gamma = M_{23}C_6 \text{ and/or } M_6C + \gamma' \text{ [10]}$$

As previously mentioned, the secondary carbides $M_{23}C_6$ and M_6C begins to form in the temperature range of 760-980 °C and 815-980 °C, respectively [10]. This was also confirmed with the JMat Pro Scheill simulation from Figure 2.2.

From studies performed by *Joseph*, it is possible to conclude that the main effect of the secondary carbides in Haynes 282 is reflected in its ductility performance [5]. The main factors that affects it are the amount of secondary carbides, their size, and specially the morphology they present. In Haynes 282, there are two main morphologies that secondary carbides can present, a continuous film along the grain boundaries, or a discrete brick-like form, as seen in Fig. 2.5.

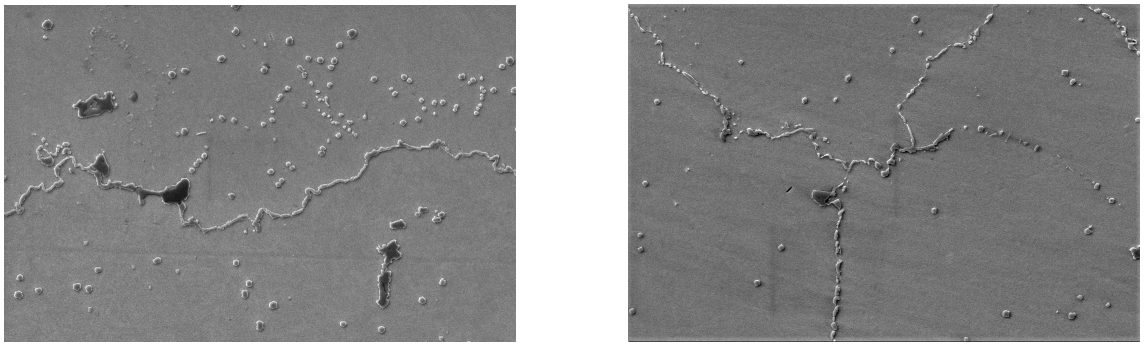

(a) Continous film (b) Discrete distribution

Figure 2.5: Grain boundary carbides distribution

From Fig. 2.5, it is possible to see the both main morphologies of secondary carbides, in which the continuous film morphology results in a decrease in ductility. On the other hand, the discrete distribution of the carbides along the grain boundary generally results in a better ductility performance, when compared to the first case. Based on literature, it is possible to predict the carbides morphology to either side, depending on the temperature of the carbide stabilization step [5]. According to *Joseph*, the main factor to define the secondary carbide distribution is the ageing temperature during heat treatment, where a low temperature below 750 °C results in a continuous film distribution, while a higher temperature would results in a discrete distribution.

A third case regarding grain boundary carbides is described by Haynes International's patent, $WO2019125637A2$, which claims that a combination of secondary

carbides and γ' precipitants along the grain boundary is the main reason of the ductility and mechanical strength improvement that is described in it [15]. According to this patent, the combined distribution along the grain boundary resulted in a ductility improvement of 14% to 100% in wrought Haynes samples; regarding the yield strength, all cases increased this property, although not as high as the increase in ductility. The main factor to achieve this distribution can be attributed to having a carbide stabilization step, during the heat treatment, below the γ' solvus temperature, which results in a bimodal distribution of the precipitate, with presence in the grain boundary. The second factor is a suitable temperature to form a discrete carbide distribution along the grain boundary, as discussed before. Both of these factors were considered for the alternatives proposed in this thesis for cast Haynes 282.

2.2.3 Heat treatment optimization

Based in the different changes in the microstructure mentioned in the last sections, GKN Aerospace designed their own heat treatment for wrought Haynes 282. In this thesis, this will now be mentioned as GKN standard heat treatment. The heat treatment consists in a multi-step heat treatment with similar objectives as the carbide stabilization and precipitation steps from Haynes standard heat treatment. GKN standard heat treatment was considered as a second reference point.

The main concern with the GKN standard heat treatment is that its design was focused in wrought version of Haynes 282. As discussed in the previous sections, there are relevant difference in the microstructure between wrought and cast Haynes 282 that variates the effect of the heat treatment, such as the dendritic structure, difference in grain size and micro-segregation, to mentioned a few. After applying the standard heat treatment in cast materials, the effects in the mechanical properties obtained by heat treatment are less relevant than the ones obtained in wrought material. The difference in ductility and strength values for cast Hayes 282 confirm the necessity of adapting the heat treatment to the cast material.

To do this, some studies have proposed different ways to improve the properties of the alloy, focusing in different steps of the heat treatment to achieve this. It is possible to categorize these methods in two main groups, the first one consists in improving the homogenization step of heat treatment, the second one focused on variation of the carbide stabilization and precipitation step of the heat treatment. The majority of these methods were designed and tested in wrought Haynes 282, but they can be translated and applied into the cast material to a certain point.

The homogenization improvement method focused on analyzing the incipient melting point of the interdendritic region of the alloy and adjusting the homogenization step temperature, usually increasing it, to reduce the segregation of Mo in this region. For this, a JMat Pro and ThermoCalc analysis must be performed to calculate the change in concentration of each element [8]. This method was studied by *Adegoke*, resulting in a hardness increase of 3% to 18%, compared to the one shown at as-cast version. The increase in hardness observed was due to the variation

of homogenization time and temperature, from 1 to 15 hours and 1050 up to 1200 °C [16]. It is important to mention that this method can be further improved by applying a multi-step treatment in the homogenization stage that may improve the mechanical properties of the alloy, as stated by *Jablonski et. Al.*.

The second method to optimize the heat treatment of Haynes 282 was the variation of time and temperature in both the carbide stabilization and precipitation steps of the heat treatment. By modifying both of these steps, the different secondary phases would present changes in their size, morphology and volume fraction, when compared to GKN and Haynes heat treatment, as mentioned in section 2.2.1. Research in literature have found that it is possible to modify the heat treatment to increase the hardness in wrought Haynes 282, as proved by *Polkowska et. Al.*, with carbide stabilization steps between 900 °C to 1100 °C combined with precipitation steps of 680 °C to 880 °C, resulting in hardness 7% higher than the one obtained with Haynes standard heat treatment [7].

There is also the case of Haynes International patent, where different time and temperature combinations were tested to improve the ductility and strength of wrought Haynes 282. This was based on three different aspects, first the modification of the carbide stabilization and precipitation temperatures, using a range of 843 - 954 °C and 704 - 843 °C, respectively; second, a time increase in carbide stabilization step from 2 hours to 4 or 6 hours; and finally, an optional step 0, consisting in the usual carbide stabilization treatment of 1010°C for 2 hours, before the alternative heat treatments proposed by the patent [15]. The purpose of these modifications is to obtain a discrete distribution of the grain boundary carbides with the addition of γ' along the same grain boundary between the secondary carbides, in order to improve both elongation and strength of the material at elevated temperatures.

Related to this study, literature also mentions the effects of single-step heat treatments in wrought Haynes 282, which has been characterized by a decrease in elongation and strength [5, 15]. The reason of the detrimental effect in mechanical properties is due to the formation of a grain boundary carbide layer and a coarser γ', in comparison to GKN and Haynes standard heat treatments. There are also studies that states the possibility of increasing the hardness of the alloy by decreasing the temperature and time of exposure in a single-step heat treatment, when ductility improvement is not the main objective [17, 18].

In this thesis, the principal way the improvement of mechanical properties are measured is through the containment factor (CF). This factor consists in the following formula: $CF = 1/2 * (YS + UTS) * (Elongation)$. The reason of using the CF to measure the improvement of the mechanical properties is its high dependence to ductility, confirming its relevance as the main objective of this study.

3

Methods

In this section it is possible to find the methodology of the different tests and analysis performed in cast Haynes 282 samples, provided by GKN Aerospace, and the conditions in which these experiments were performed.

3.1 Cast Haynes 282 samples

The cast Haynes 282 material, provided by GKN Aerospace, consisted of two cast plates produced by investment casting, each one with different dimensions. The dimensions of the first plate were 300 mm x 130 mm x 20 mm, while the second plate presented dimensions of 300 mm x 60 mm x 13.5 mm. These plates were used for three sample batches, each one for different purposes. One batch was heat treated and used for hardness testing, followed by microstructure analysis. A second batch was heat treated at GKN facilities and sent for machining to an external lab, for tensile testing. The third batch consisted in samples used for an additional study regarding the microstructural changes during the carbide stabilization step.

3.1.1 Sample preparation

The process to obtain the batch of samples that were used for hardness and microstructure characterization consisted first in cutting out 16 cubes of each plate, 32 in total. The cubes had the dimensions of 20 mm x 20 mm x 20 mm from the first plate and 13.5 mm x 13.5 mm x 13.5 mm from the second. For this, the plate went through an electrical discharge machining (EDM) process. Studies were performed before and after mounting, grinding and polishing of the material for comparison purposes.

The samples used for tensile test were prepared differently, in which 6 blocks were cut from each cast plate via EDM. The dimensions of the blocks variated depending if they came from the 20 mm thickness plate or the 13.5 mm thickness plate, having dimensions of 78 mm x 56 mm x 20 mm and 78 mm x 19 mm x 13.5 mm, respectively. After the blocks were heat treated with their corresponding parameters, they were machined and tested according to ASTM E8 for tensile test specimens. The machining of the tensile test samples was performed at an external laboratory, where the tensile tests were also performed.

For the carbide stabilization step study, 3 cube samples were machined out of the 20 mm thick plate, with dimensions of 20 mm x 20 mm x 20 mm, via EDM. Similar to the other cube sample batch, studies were performed before and after mounting, grinding and polishing.

3.2 Heat treatment selection

For the heat treatment selection, the different studies from literature mentioned in section 2.2.3 were analyzed and adapted to the sample availability at GKN. The selected heat treatment consisted in 15 options, presenting variations in time, temperature, and number of precipitation steps. The main modifications of the heat treatment parameters are described for each of them, taking as a reference the standard heat treatment recommended by Haynes International. The cast plates were received after HIP and solution treatment. Considering the as-received conditions of the plates, the samples were heat treated with carbide stabilization and precipitation steps only.

Heat treatments proposals:

- Haynes standard: Reference heat treatment - 1010 °C / 2 hrs + 788°C / 8 hrs
- GKN standard: Multi-step heat treatment with carbide stabilization and precipitation steps
- 1-step: Single step with higher temperature in precipitation step
- HT1: Increased time in carbide stabilization step
- HT2: Decreased time in precipitation step
- HT3: Increased temperature in carbide stabilization step
- HT4: Increased temperature in carbide stabilization step, decreased temperature in precipitation step
- HT5: 3-step heat treatment based in René-41 alloy
- HT6: Increased time and decreased temperature in carbide stabilization step
- HT7: Increased time and decreased temperature in carbide stabilization step, decreased time in precipitation step
- HT8: Addition of Step 0, increased time and decreased temperature in carbide stabilization step
- HT9: Increased time and decreased temperature in carbide stabilization step, decreased temperature in precipitation step
- HT10: Increased time and decreased temperature in carbide stabilization step
- HT11: Increased time and decreased temperature in carbide stabilization step, decreased temperature in precipitation step
- HT12: Addition of Step 0, increased time and decreased temperature in carbide stabilization step

These heat treatments were applied to the 32 cube samples described in 3.1.1 using a laboratory muffle furnace. The furnace used for this did not possess controlled cooling, all samples were air cooled (AC) after each step of the heat treatment.

The purpose of these heat treatments was to analyze and compare the different variations of each step and their effect in the microstructure, having as a reference Haynes standard heat treatment, followed by GKN standard heat treatment. In different heat treatments, such as HT6 and HT10, the objective was to see the effect of varying temperature in the carbide stabilization step. On the other hand, heat treatments HT9, HT10 and HT11, had as a main objective the analysis of the microstructural changes by modifying time and temperature in the precipitation step. Heat treatments HT2 and HT7 were included to analyze the effect of reducing the time during the precipitation step. Lastly, heat treatments HT8 and HT12 were used to see the changes by adding a Step 0 before the alternative heat treatment.

3.2.1 Cooling rate

As mentioned in the previous section, the heat treatments performed in the cubic samples, as well as in the carbide study samples, did not present a controlled cooling rate between steps. Instead, the samples were taken out and cooled via air cooling until room temperature was reached.

In order to measure the cooling process the samples were subjected to, two K-type thermocouples were instrumented into additional cubic samples for the purpose of recording the temperature after being taken out of the furnace. The embedded thermocouples can be observed in Fig. 3.1, with a thickness of 20 mm and 13.5 mm each one, containing the thermocouple at the center of the sample.

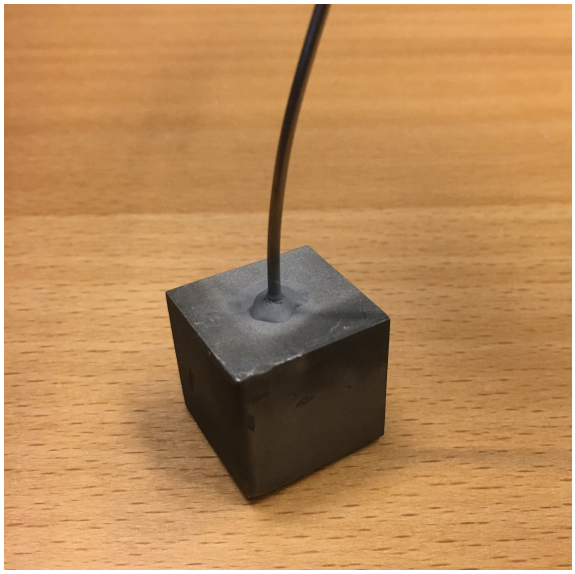

Figure 3.1: Instrumented sample with thermocouple

Both sensors were subjected to a heat treatment of 30 minutes at different temperatures. The first cycle the thermocouples were subjected to was at 1065 °C, while a second cycle of 30 minutes was performed at 650 °C. A 1 Hz sampling was performed, which was the highest frequency allowed by the thermocouple. With the values obtained, a general cooling rate was calculated using the required time to reach a temperature of 590 °C, which is a parameter that is commonly used in production processes.

The results obtained were compared with the cooling rates measured from the production furnace, which were used for the tensile test specimens. In addition to this, they were compared to the cooling rate from the solutionizing process that the as-received material went through before the heat treatment.

3.3 Hardness test

For the hardness analysis, the experiments were divided into three phases, one for the cubic samples that received the 16 different heat treatments, a second phase focused on the heat treated blocks that were used for tensile testing, and a third phase for the carbide stabilization study samples. This division was due to the different conditions and purpose each sample presented.

The first phase of experiments was also divided into two steps, one focused on the cube samples in conditions just after heat treatment, and the second step focused on selected samples that were mounted, ground, and polished. Besides the cubic samples that were analyzed for each heat treatment alternative, an additional as-received solutionized sample was included for reference comparison. In the first step, a Rockwell C indentation was decided to be used, based in the expected hardness values of the samples. After the first test, the most representative heat treatments were selected based in the hardness values they presented. The selected heat treatments (Haynes standard, GKN standard, HT1, HT5, HT6, HT10, HT11, HT12) were mounted for the second hardness analysis. Simultaneously, the hardness values were found to be in the lower end of the Rockwell C scale, leading to a change in methodology for the second analysis, now using macro-Vickers in the mounted samples. The values recorded in Rockwell C scale were converted to HV units according to the ASTM E140-12b standard for hardness conversion. A comparison between the two analysis were done, for the purpose of analyzing the change in hardness between the cube sample surface and its center. This was done for samples with both 20 mm and 13.5 mm thickness.

The second phase of the hardness tests was performed in the blocks that were heat treated for tensile tests. As mentioned before, these blocks were cut and heat treated before being machined for tensile testing, which limited the hardness test that could be performed. The blocks could only be tested with Rockwell C indentation at their surface, with no macro-Vickers measurement at the center. Due to furnace availability, it was possible to measure the hardness before and after heat treatment, which allowed the calculation of hardness increase percentage post-heat treatment. Similar to the first phase hardness analysis, this was done in blocks with both thicknesses.

The third phase's objective was to analyze the hardness change in the samples subjected to different carbide stabilization temperatures. The purpose of this test was to confirm the variation of γ' precipitates at different temperatures above its theoretical solvus temperature of 997 °C. The hardness analysis was similar to the cube samples mentioned before, with a first step using Rockwell C indentation in the cube surface, followed by a macro-Vickers test after mounting. The values recorded in Rockwell C scale were also converted to HV units according to the ASTM E140-12b standard for hardness conversion for comparison between each region.

3.4 Microstructure analysis

The plan for the microstructure analysis consisted of first analyzing the hardness values found in the 32 cube samples and based on that select the samples that presented maximum, minimum and relevant results for the analysis. Besides that, it was decided to have the as-received sample, the Haynes and GKN standard heat treated samples as reference for comparison with the other heat treatment alternatives. As mentioned in section 3.1.1, the selected samples and references were mounted, ground, and polished accordingly to Buehler SUM-MET guide for samples preparation. This step was followed by an iterative etching process until the best condition was achieved. The samples that were prepared for microstructure analysis were: As-received, Haynes standard, GKN standard, HT1, HT5, HT6, HT10, HT11, and HT12. Additional to the selected samples based in hardness results, the same preparation process was used for the 3 carbide stabilization samples.

The samples were first analyzed in an optical microscope in a pre-etched condition for defects analysis. After etching, the samples were analyzed in the same microscope for general analysis at low magnification, from x25 to x500. For high magnification analysis, two SEM analysis were performed, one using an EVO-HD25 SEM for low magnifications, and an Zeiss Ultra-55 for high magnification. These were used to identify the main secondary phases present in the material. Special interest was aimed towards the grain boundary morphology and γ' precipitates size and fraction, for their characterization.

3.4.1 Etching

The etching process for the samples that were selected for microstructure analysis, including the carbide stabilization study samples, received an iterative etching process until the ideal conditions were met for both optical microscopy and SEM. In total, the process consisted in three iterations with a microstructure review between them, in which the main objective was to improve the resolution of γ' at high magnification.

The first trial that was performed consisted in an electrolytic etching of 100 ml HCl + 0.5 ml H_2O_2 with 5V for 6 seconds. The results obtained with it did not match the expected resolution in SEM, so a different etchant was selected. For the second iteration, an electrolytic etching with oxalic acid 10 gr + 100 ml H_2O with 3 V for 20 seconds was selected . In this iteration the quality of the image was improved.

A third trial was done using the same oxalic acid etchant, this time using 2.5 V for 20 seconds. The images obtained were substantially improved for SEM analysis, concluding the etching iterations.

3.5 Tensile test

In order to confirm the improvement in ductility, yield, and tensile strength properties of cast Haynes 282, a tensile test was performed in selected heat treatments, including 2 heat treatment references and 4 alternative ones. The testing was performed at both room temperature (RT) and at elevated temperature, 750 °C.

3.5.1 Heat treatment for tensile test

The heat treatment selection for tensile test was based in several factors that considered literature studies, JMat Pro and Thermo-Calc simulations, and hardness values from the cube samples. The heat treatments selected were: Haynes standard, GKN standard, HT1, HT10, HT11, and HT12, with the first two working as a reference for the proposed alternative heat treatments.

3.5.2 Tensile test

The mechanical tensile test was performed at an external laboratory, where the heat treated blocks were machined and tested. The machining process followed the standard drawing for tensile specimens. The applied heat treatment per block and the test environment conditions can be observed in Table 3.1. It is important to specify that from the 3 samples tested at RT, two are from the 20 *mm* thick block, and one comes from the 13.5 *mm* block; both samples tested at elevated temperature come from the 20 *mm* block.

Table 3.1: Tensile test conditions and specifications

Heat treatment ID	No. of Samples @ RT	No. of Samples @ 750 °C
Haynes standard	3	2
GKN standard	3	2
HT1	3	2
HT10	3	2
HT11	3	2
HT12	3	2
Total	18 samples	12 samples

Testing was carried out following the ASTM E8 standard for tension testing, and ASTM E21 standard for elevated temperature tension testing. In both cases, the test was carried on in air environment, and consisted in a strain control tensile test, which strain rate was 0.005 mm/mm gage length per minute up to yield stress, then 0.05 mm/mm gage length per minute. The tests were carried out until rupture.

3.6 Carbide stabilization study

Regarding the carbide stabilization step study mentioned previously, 3 samples were subjected to different temperatures for a period of 2 hours. The purpose of this experiment was to analyze the microstructural effects the first step of the heat treatment has on the material. The different parameters used can be observed in Table 3.2.

Table 3.2: Heat treatments for carbide stabilization study

Heat treatment ID	Carbide stabilization
CS1	1065 °C - 2 hrs.
CS2	1010 °C - 2 hr.
CS3	900 °C - 2 hr.

The three different temperatures were selected in order to test the main stages in which secondary carbides present in the material. The temperature for CS1, 1065°C, was chosen to analyze the degree of solutionizing that is achieved at this temperature, with the solvus temperature of both γ' and secondary carbides below it. The temperature chosen for the second sample, 1010 °C, is the usual carbide stabilization step used for the standard heat treatment recommended by Haynes International. The purpose of this sample is to confirm the dissolution of γ' at this temperature, due to some studies in literature claiming its solvus temperature is above 997 °C. The temperature chosen for the third sample, 900 °C, was chosen to analyze the behavior of γ' while precipitating since the carbide stabilization step; something that is expected for several heat treatments considered. Similar to the heat treatment of the cube samples, the heat treatments were performed in a laboratory furnace with no controlled cooling rate, going through AC after the process.

The analysis performed in these samples consisted in hardness test, SEM and image analysis through MIPAR software.

4

Results

In this section it is possible to find the results of the different tests described in section 3. The section is divided into simulations, cooling rate experiments, hardness tests in different conditions, microstructure analysis results, tensile tests results, and the additional carbide stabilization study results.

4.1 γ' Simulations

As mention in section 2, the results obtained from the simulation presented similar values observed in literature. In the simulations, γ' had a size of 27.4 nm and a volume fraction of 17% , while the experimental data presented an approximated size of 20 nm and a volume fraction of 20 % for wrought Haynes 282 [13, 14]. For cast versions of the material, the experimental data from *Matysiak et. Al.* showed bi-modal precipitants with spherical 74 nm γ' with a volume fraction of 9.6 % in the dendritic structure, and a cubic 113 nm γ' with a volume fraction of 8.5 % in the interdendritic region.

After the base simulation, different simulations were performed with variations of the precipitation step during the heat treatment. The reason the carbide stabilization step was not modified is that a state of complete γ' dissolution was assumed. The results obtained from these JMat Pro simulations can be observed in Table 4.1.

Table 4.1: Simulations for precipitation time variation - Constant carbide stabilization step

Carbide stabilization step	Precipitation step	γ' size [nm]	γ' volume fraction [%]]
1010 °C - 2 hours	788 °C - 2 hours	21.99	17
1010 °C - 2 hours	788 °C - 4 hours	24.08	17
1010 °C - 2 hours	788 °C - 8 hours	27.41	17
1010 °C - 2 hours	788 °C - 16 hours	32.18	17

From Table 4.1, it is possible to see that the main γ' characteristic that is being affected is its size, in which more time represents more γ' growth. By taking the example of reducing the precipitation time at 788 °C, from 8 hours to 4 hours, the size of γ' goes from 27.43 nm to 24.08 nm. The same effect occurs for all the temperatures simulated, below γ' solvus temperature, where time is changed.

Table 4.2: Simulations for precipitation temperature variation - Constant carbide stabilization step

Carbide stabilization step	Precipitation step	γ' size [nm]	γ' volume fraction [%]]
1010 °C - 2 hours	730 °C - 8 hours	21.92	19
1010 °C - 2 hours	760 °C - 8 hours	23.62	18
1010 °C - 2 hours	788 °C - 8 hours	27.41	17
1010 °C - 2 hours	850 °C - 8 hours	45.67	14

In Table 4.2, the parameter that was now studied was the variation of temperature in the precipitation step of the heat treatment. The selected values were based on a Haynes International patent, $WO2019125637A2$, where different heat treatments were selected to improve mechanical properties of wrought Haynes 282 [15]. The results obtained from the JMat Pro simulations indicate that the variation of the precipitation step temperature affects both size and volume fraction of γ' precipitate, unlike just the variation of the time. In this case, the increase of temperature from 730 °C to 850 °C is reflected in the increase in γ' size and simultaneously the decrease of its volume fraction in the microstructure, from 19 % to 14 %.

Table 4.3: Simulations for carbide stabilization temperature variation - Constant precipitation step

Carbide stabilization step	Precipitation step	γ' size [nm]	γ' volume fraction [%]]
850 °C - 2 hours	788 °C - 8 hours	35.93	17
900 °C - 2 hours	788 °C - 8 hours	55.17	17
930 °C - 2 hours	788 °C - 8 hours	78.09	17
950 °C - 2 hours	788 °C - 8 hours	102.17	17

Finally, the last set of simulations performed focused in the variation of temperature of the carbide stabilization step, assuming it is below the γ' solvus temperature. The results obtained can be observed in Table 4.3. As in the previous simulation, the temperatures used in the simulation were based in Haynes International's patent [15]. The results obtained show that γ' volume fraction is not affected by the variation of the carbide stabilization step temperature, but its size does change drastically, with a range of almost 100 nm when variating the temperature from 850 °C to 950 °C. The complete set of simulations are presented in Appendix 1, with results of size and volume fraction of γ' for different combinations of time and temperature.

4.2 Cooling rate

As mentioned in section 3.2.1, the cooling rates were obtained for the different processes the material went through. These rates were obtained directly from the furnace records. For the solution treatment process that the material went through before arriving to GKN, the cooling rate was 0.866 °C/sec. On the other hand, the samples that went through heat treatment in a production furnace, presented a cooling rate of 0.35 °C/sec at the highest temperatures present in the carbide stabilization step, and a cooling rate of 0.37°C/sec in the precipitation step, at lower temperatures.

The cooling rate for the heat treatments applied in the cube samples were measured using a thermocouple embedded sample at two temperatures, 1065 °C and 650 °C, resulting in the cooling curves shown in Fig. 4.1. As expected, the cooling process for the 13.5 *mm* thick samples occurs at a higher rate than the 20 *mm* thick samples in both cases. In order to compare the measured rates with the ones mentioned previously, the rate between the highest temperature, either 1065 °C or 650 °C, and 590 °C was calculated. For the 1065 °C case, the sample reached 590 °C degrees in 150 seconds for the thick sample and 102 seconds for the thin sample, resulting in a cooling rate of 3.11 °C/sec and 4.58 °C/sec respectively. For the 650 °C case, the samples presented a cooling rate of 1.29 °C/sec in the 20 *mm* thick sample, and 3 °C/sec in the 13.5 *mm* thick sample. The importance of these values was expected to be reflected in the precipitation of secondary phases in the material, which will be analyzed in the following sections.

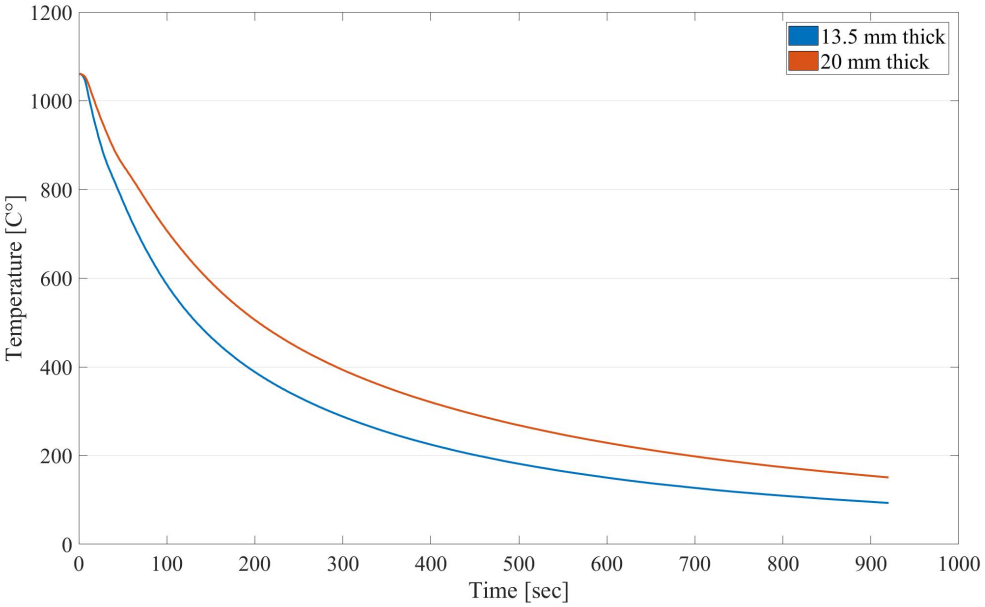

(a) Starting temperature - 1065 °C.

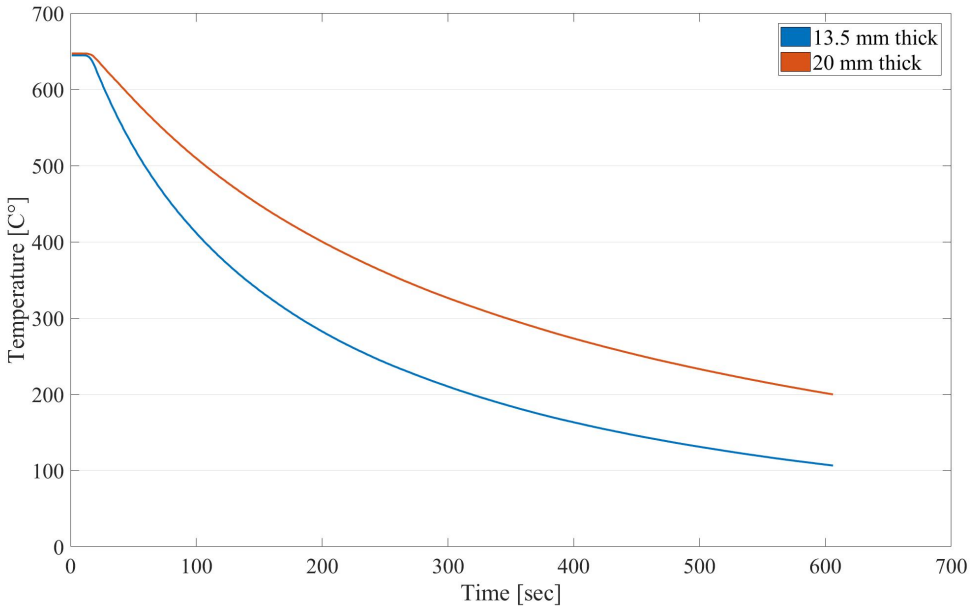

(b) Starting temperature - 650 °C.

Figure 4.1: Experimental cooling rate.

4.3 Hardness test

As mentioned in the previous section, the hardness evaluation of the heat treated samples were divided in two categories due to the different conditions during heat treatment, one analysis for the cubic samples and one for the blocks that were used in the tensile test.

4.3.1 Hardness - Cube samples

Hardness values were measured from the cube samples in two phases, the first one consisted of measuring the values at the surface, followed by a measurement in the center of the samples. The results obtained can be observed in Fig. 4.2, for both thicknesses. In these figures it is possible to see the change in hardness compared to the as-received solutionized sample. In the as-received sample, the hardness observed presented values similar to a heat treated material, which may indicate the presence of γ' since this step. Another effect that was observed is the lack of hardening in some heat treatments, which occurred in both 13.5 mm and 20 mm thick samples.

There is a difference in hardness between the sample surface and its center region, with a higher value present in the later one. The increase in hardness between surface and center varies from 4 % to 14 % depending on the heat treatment. The reason of the difference between the regions is attributed to: cooling rate change between center and surface, solute segregation effect that is reflected in a difference in γ' distribution, or variation in test methods between regions. This phenomena was studied further in the carbide stabilization step study.

It is important to note that the values shown in Fig. 4.2 are only the heat treatments that were tested for tensile test, in addition to the maximum and minimum hardness values observed. The complete set of hardness values can be found in Fig. A.1, in the Appendix of this report.

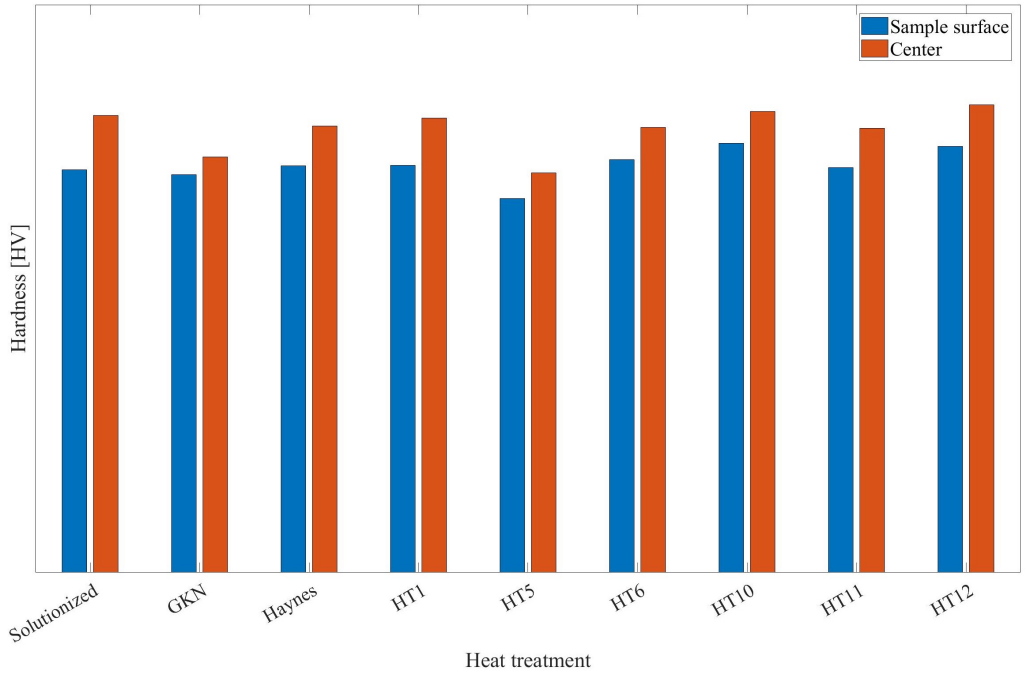

(a) Hardness comparison - 20 mm thick

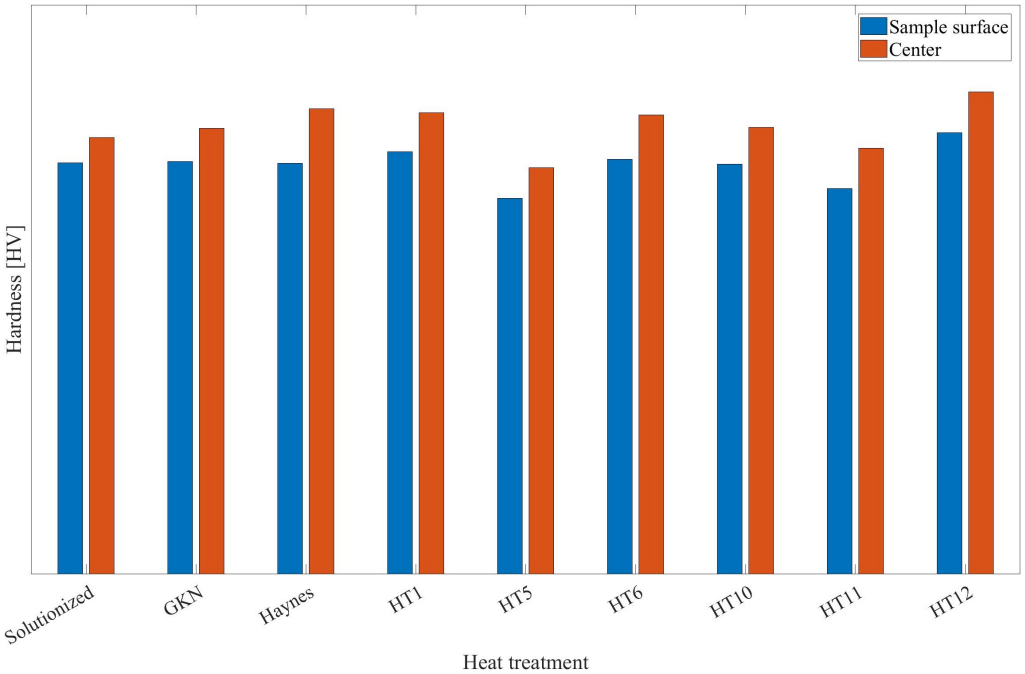

(b) Hardness comparison - 13.5 mm thick

Figure 4.2: Hardness comparison in selected samples

4.3.2 Hardness - Block samples for tensile test

The heat treated blocks that were sent for tensile test went through a hardness measurement before and after heat treatment, for both the 13.5 *mm* and 20 *mm* thick blocks. The hardness values obtained can be observed in Fig. 4.3. Unlike the previous section, these values come exclusively from the block surfaces.

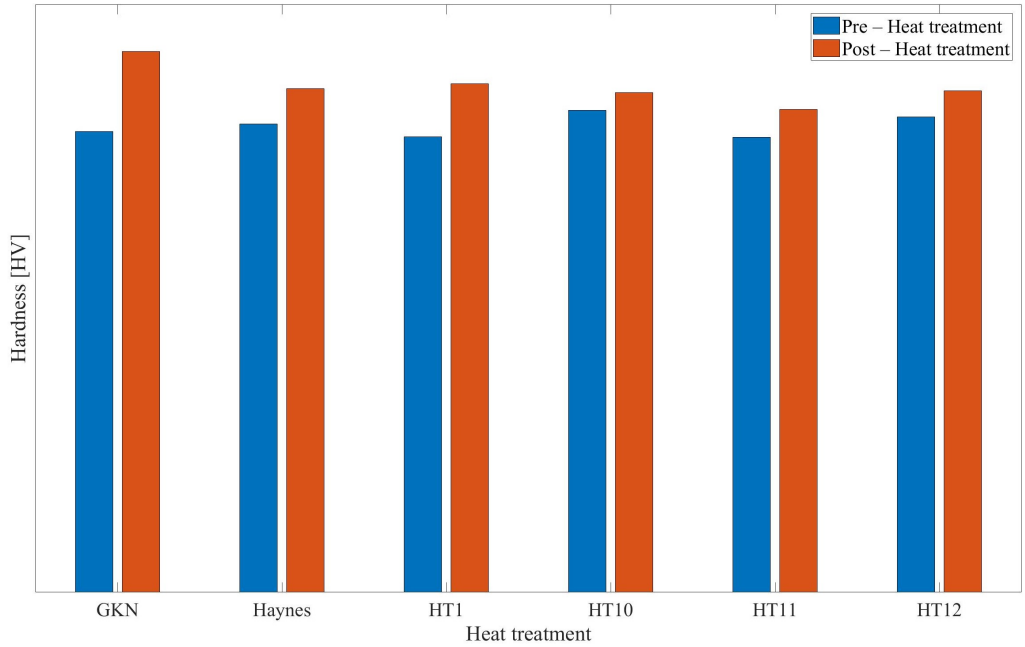

(a) Hardness comparison - 20 mm thick

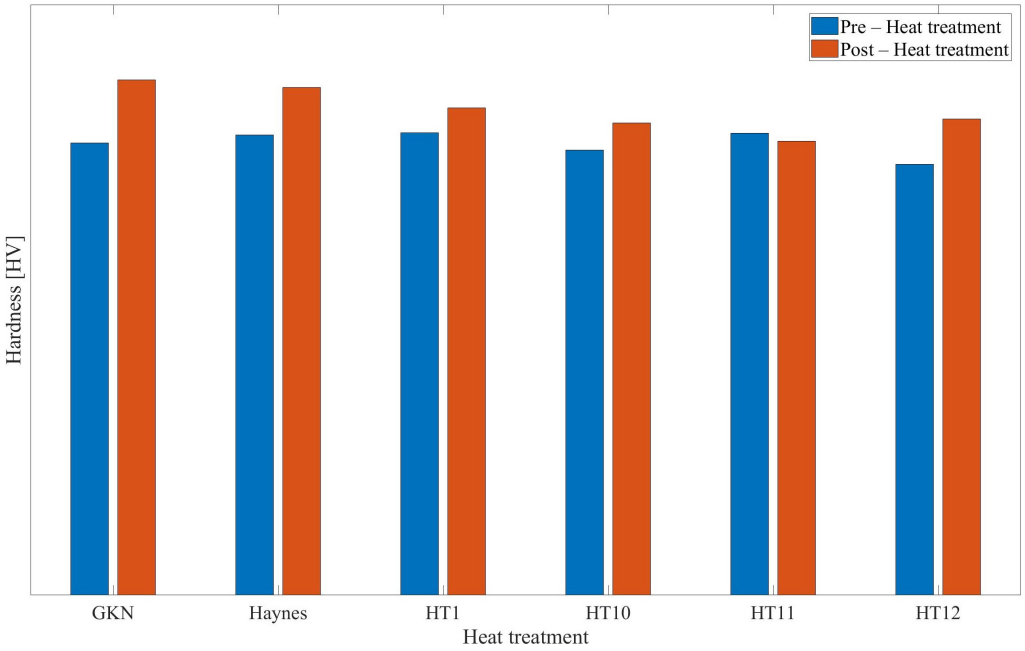

(b) Hardness comparison - 13.5 mm thick

Figure 4.3: Hardness - Before and after heat treatment

In order to analyze the change of hardness due to the heat treatment, Fig. 4.4 shows the change in percentage for each block. GKN standard heat treatment shows the highest increase, while other alternatives, such as HT10 and HT11, show a slight increase or even decrease in hardness.

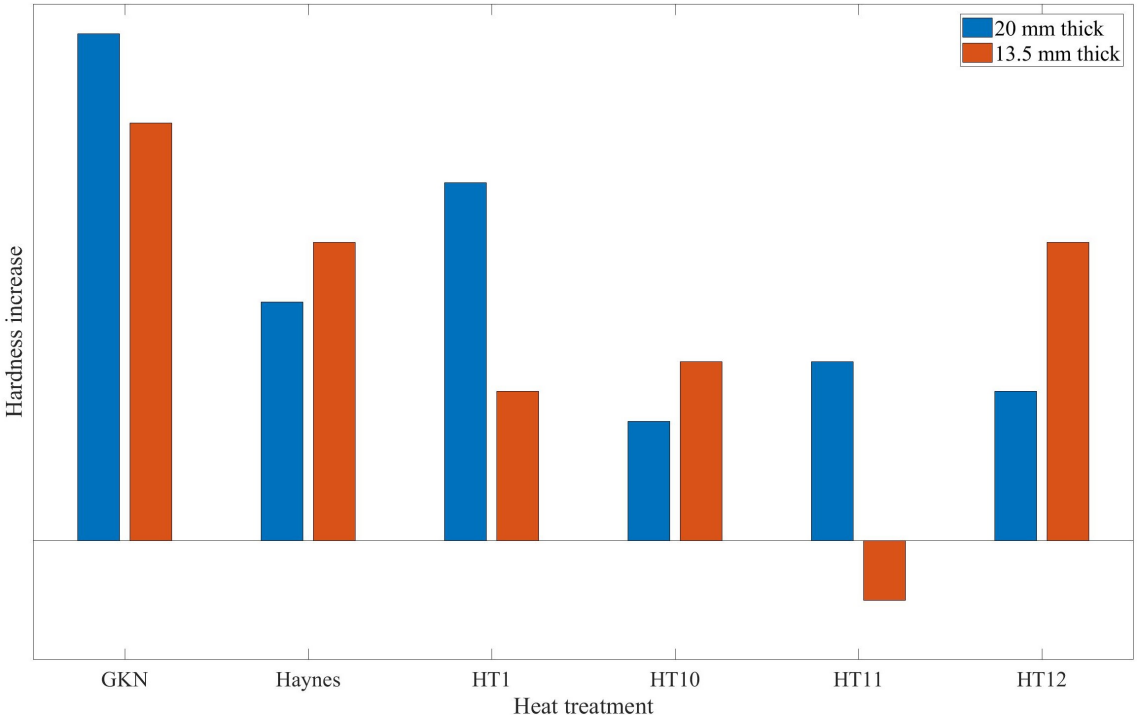

Figure 4.4: Hardness increase - Block samples

4.4 Microstructure analysis

The microstructure analysis of the different samples after heat treatment was carried out in two main studies. The first study consisted of using optical microscopy with the main objective of analyzing the grain boundaries and presence of secondary carbides. The second study was an SEM analysis of the samples, with special attention on identifying secondary carbides and analyzing γ' in order to characterize its size and distribution in the different samples.

4.4.1 Optical microscopy

The initial results of the optical microscopy analysis showed differences in the microstructure caused by each heat treatment. In these results a dendritic structure was observed in all the samples, with difference in its size depending on the heat treatment they went through. In Fig. 4.5 it is possible to see some general differences between the samples at low magnification. It is important to note how the etching also changed between samples, causing a difference in how the grain boundaries and the dendritic structure looks.

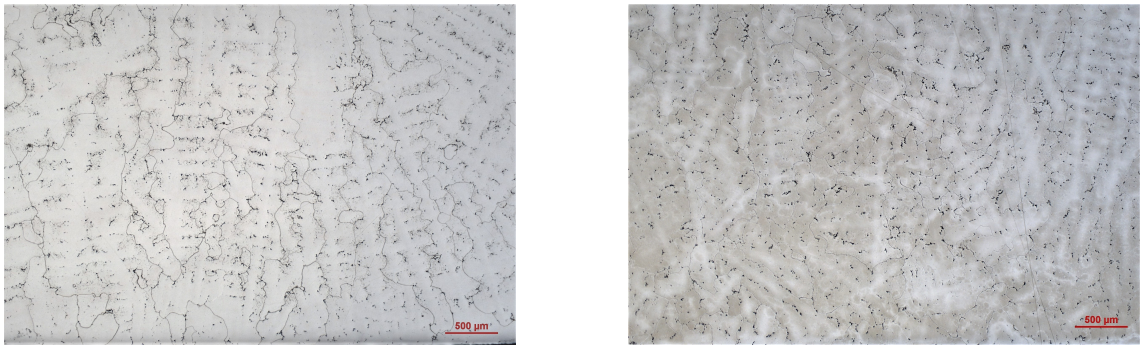

(a) GKN standard - x2.5

(b) HT12 - x2.5

Figure 4.5: Optical microscopy of heat treated samples - Low magnification comparison

When analyzing the microstructure at high magnification, as shown in Fig. 4.6, a clearer difference between heat treatments can be observed. Not only the grain size changes between the sample, but also the remaining solute segregation in the inter-dendritic regions. Some samples, such as HT11 and HT12, show a cleaner microstructure inside the grains, while others show a more pronounced dendritic structure, which is the case of GKN standard and HT1 heat treatments. These initial observations had to be confirmed with the SEM analysis, but served as an initial point for the microstructure analysis.

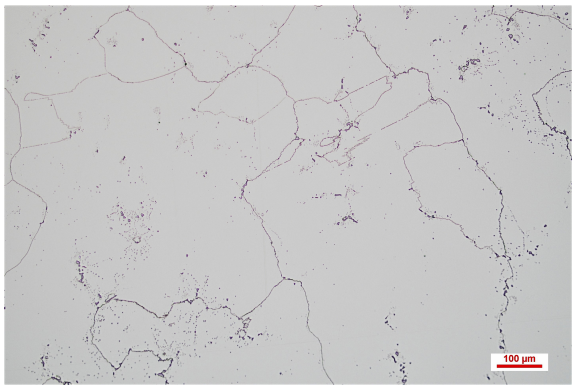

(a) Haynes standard - x10

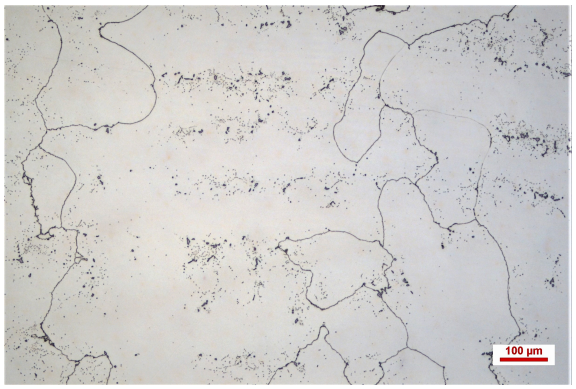

(b) GKN standard - x10

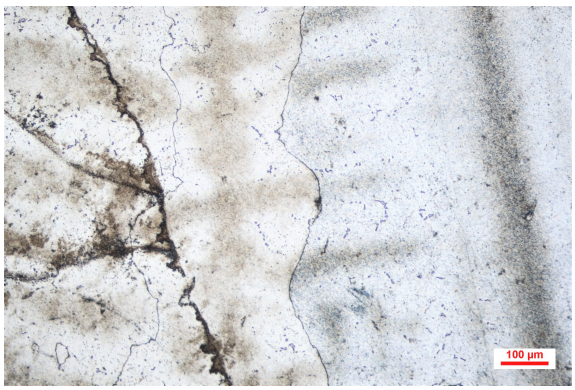

(c) HT1 - x10

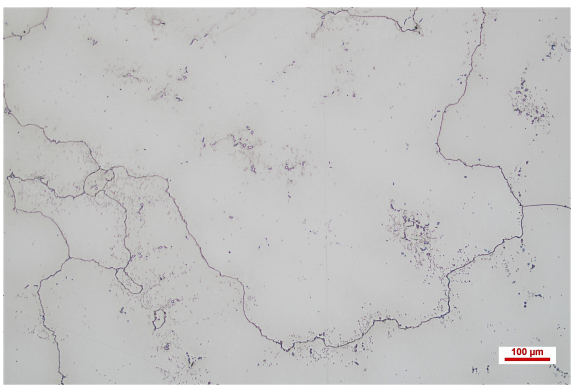

(d) HT10 - x10

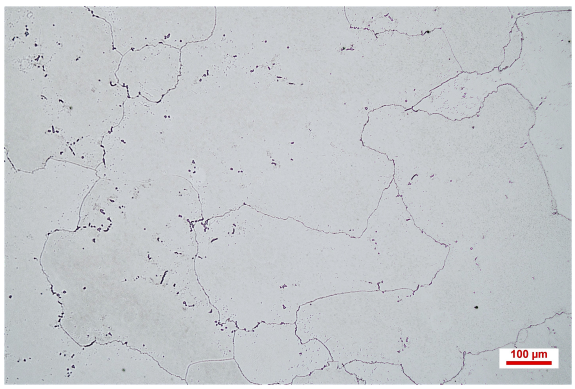

(c) HT11 - x10

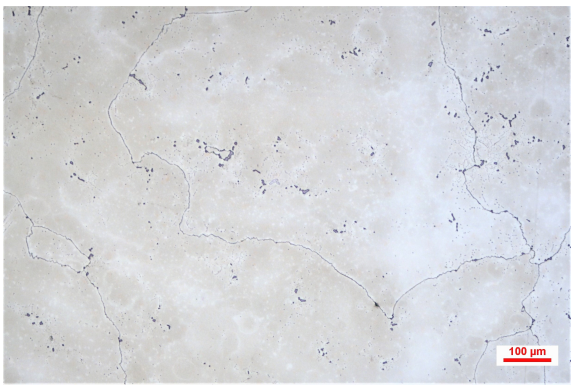

(d) HT12 - x10

Figure 4.6: Optical microscopy of heat treated samples

4.4.2 Scanning Electron Microscopy - SEM

After completion of the optical microscopy analysis, the samples were analyzed through SEM in order to identify the carbides that were present in their microstructure. Simultaneously, the γ' precipitates were analyzed for the purpose of characterizing their size and distribution.

The first sample to be analyzed was the as-received condition, in which an initial solution treatment had taken place and was not modified by the activities that were carried out in this project. The microstructure in this condition shows an almost fully precipitated material, as seen in Fig. 4.7. There is evidence of secondary carbides and blocky grain boundary carbides in it. Fig. 4.7b clearly shows the γ' precipitated in the matrix.

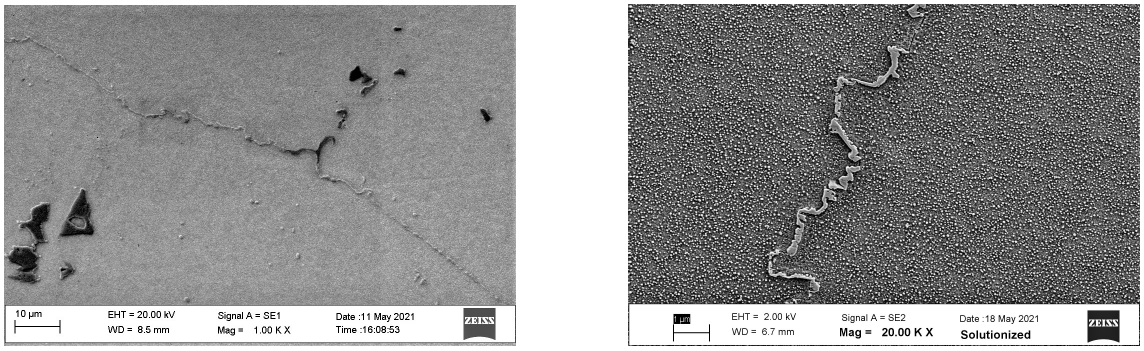

(a) Grain boundary carbides (b) γ' + carbides

Figure 4.7: SEM analysis - As-received sample

The SEM analysis of Haynes standard heat treatment showed a fine γ' dispersion in the matrix, with low variation of size within its microstructure. It is also possible to observe in Fig. 4.8a secondary carbides present in the sample, and a continuous grain boundary layer that was present.

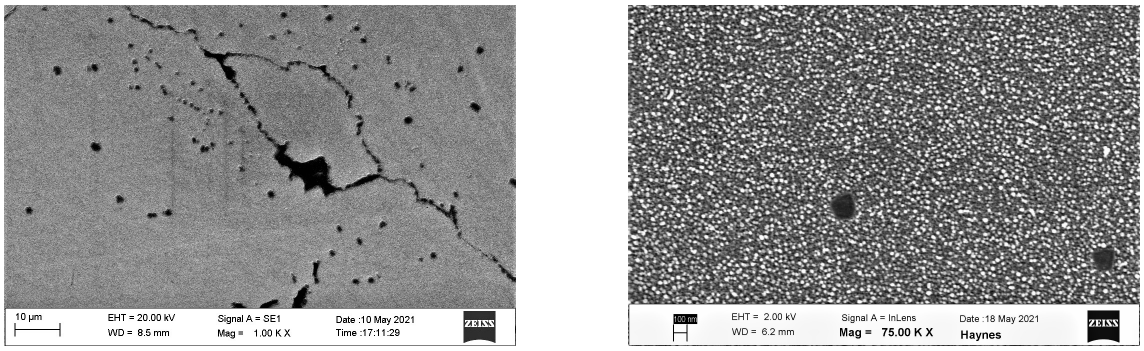

(a) Grain boundary carbides (b) γ' + carbides

Figure 4.8: SEM analysis - Haynes standard heat treatment sample

For the GKN standard heat treatment sample, the microstructure observed is shown in Fig. 4.9. There, it is possible to see the distribution of secondary carbides both at the grain boundaries and inside the grain. The γ' observed in 4.9b shows a bimodal size distribution, in which fine precipitates are spread in the matrix, and bigger γ' with clear spherical morphology are found within them. Regarding its grain boundary morphology, a mostly continuous carbide layer was observed in the sample.

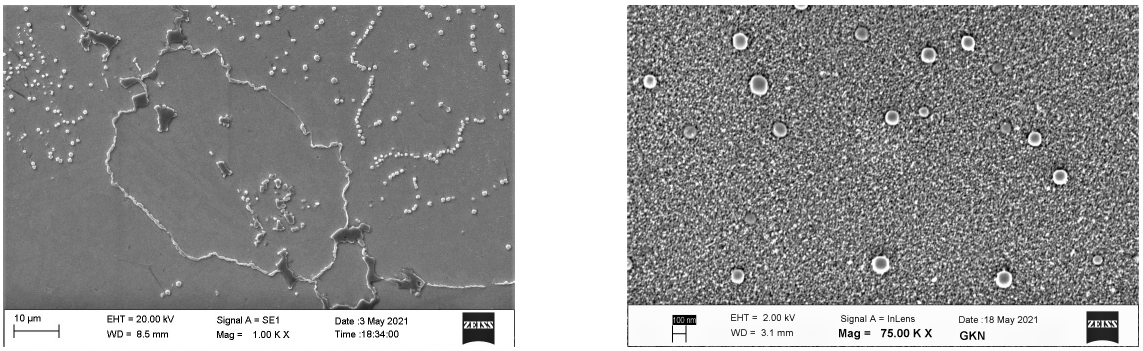

(a) Grain boundary carbides (b) Bimodal γ' (High mag.)

Figure 4.9: SEM analysis -GKN standard heat treatment sample

The microstructure observed in HT1 sample, Fig. 4.10, presented similarities with Haynes standard sample. In these samples, the secondary carbides and γ' size and distribution was similar to Haynes standard, with bimodal size and a continuous grain boundary.

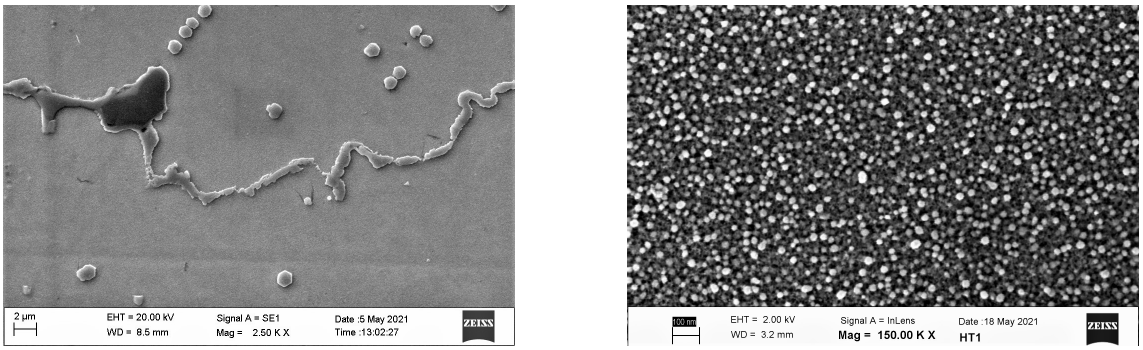

(a) Grain boundary carbides (b) γ' (High mag.)

Figure 4.10: SEM analysis - HT1 sample

For HT10 microstructure, a bigger difference can be observed compared to the previous samples. In Fig. 4.11, it is still possible to see a continuous grain boundary layer, but now the precipitation of γ' resulted in bigger particles. The high magnification images in this sample show clearly this result.

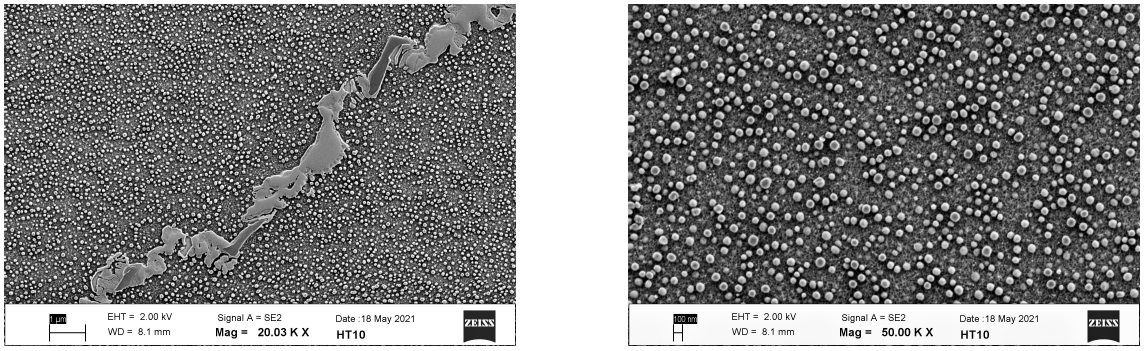

(a) γ' + carbides (b) γ' (High mag.)

Figure 4.11: SEM analysis - HT10 sample

In Fig. 4.12, HT11 microstructure shows also a bigger γ' distribution in its matrix, similar to HT10. The main difference between these two is in the volume fraction, in which HT11 shows less precipitation of γ'. It is important to note that the grain boundaries has also a continuous morphology.

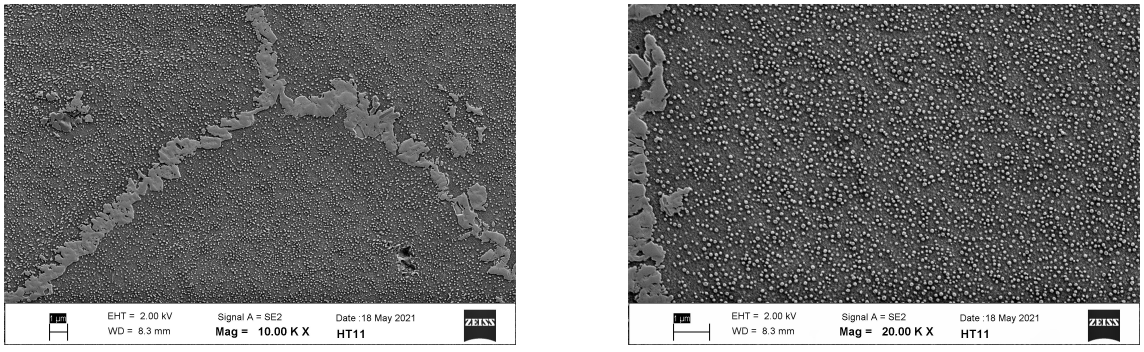

(a) γ' + carbides (b) γ' (High mag.)

Figure 4.12: SEM analysis - HT11 sample

The final samples analyzed was HT12, in which microstructure is showed in Fig. 4.13. As seen in the last two heat treatment alternatives, the γ' present in the sample is bigger than the reference heat treatments, Haynes and GKN standard, but secondary carbides distribution is still similar.

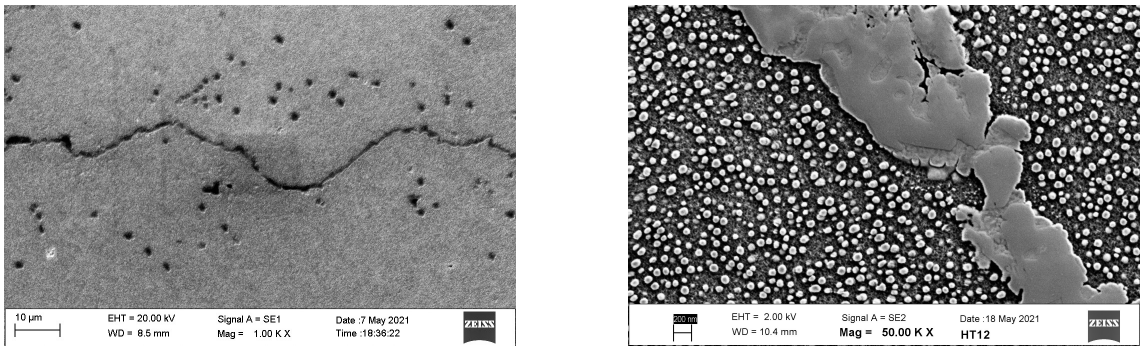

(a) Grain boundary carbides (b) γ' (High mag.)

Figure 4.13: SEM analysis - HT12 sample

4.4.2.1 Gamma prime γ' analysis

After the SEM study, image analysis for γ' characterization took place based on the images obtained. The first sample to be studied was the as-received solutionized sample, in which main objective was to confirm the full precipitation of the material. In Fig. 4.14, the size distribution of γ' is shown, with a size well above 20 nm.

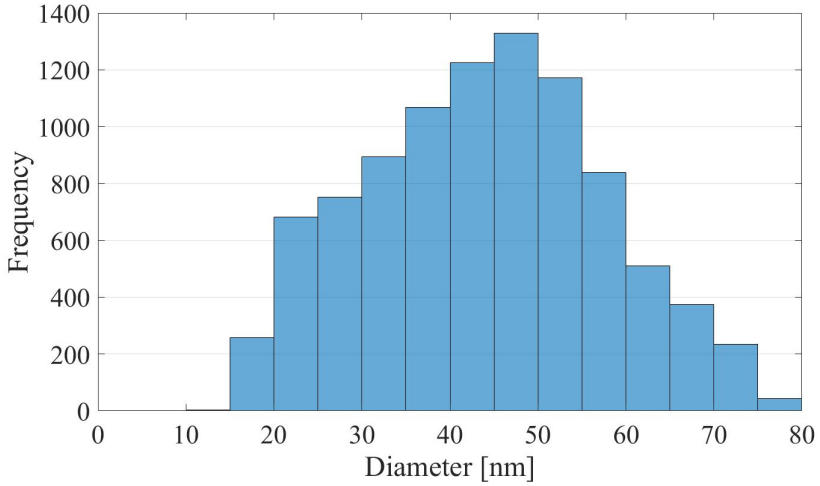

Figure 4.14: Gamma prime γ' size distribution - As-received condition

The size distribution for the rest of the samples, including the reference Haynes and GKN standard heat treatment, can be observed in Fig. 4.15. In it, the effects of each heat treatment on the precipitation of γ' are shown.

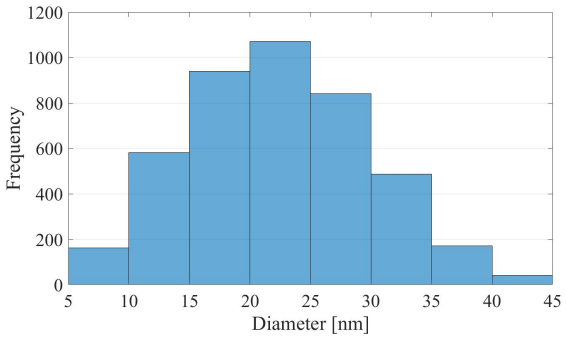

(a) Haynes standard

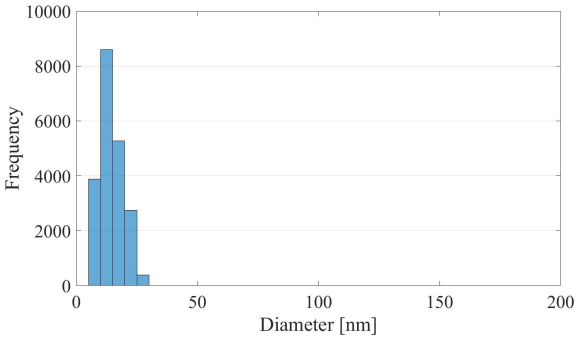

(b) GKN standard

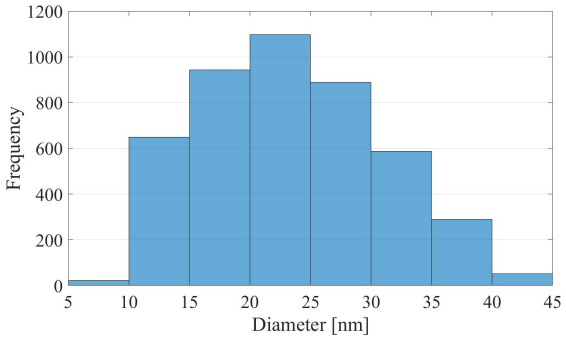

(c) HT1

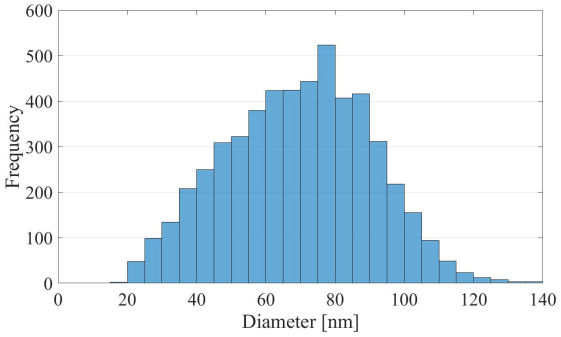

(d) HT10

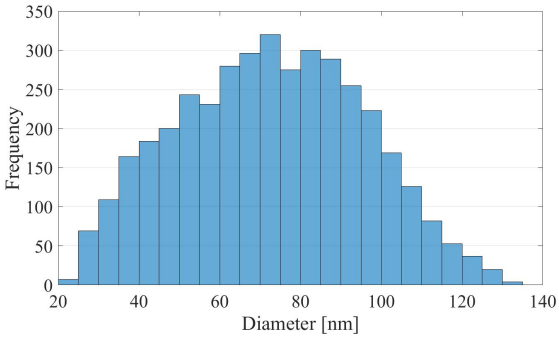

(c) HT11

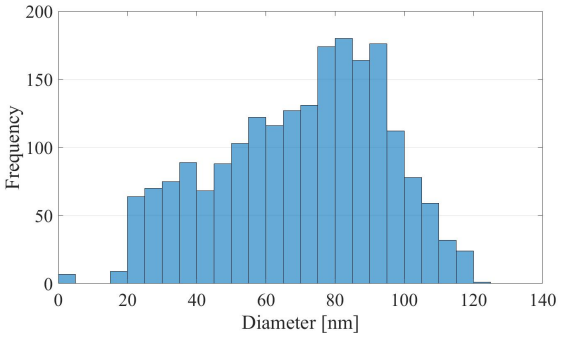

(d) HT12

Figure 4.15: Gamma prime γ' size distribution

In order to have a better understanding of the distribution of each heat treatments, in Fig. 4.16 is possible to see each size distribution together for comparison reasons. It is important to note the addition of the as-received solutionized condition, that serves as a common initial point for all heat treatments.

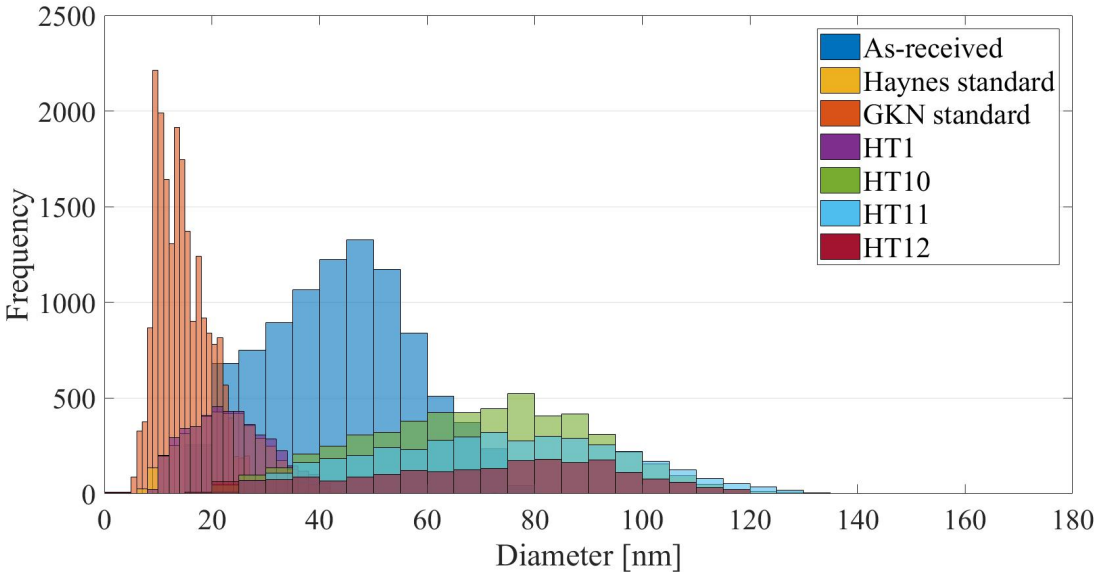

Figure 4.16: γ' size distribution for all heat treatments

To summarize the values obtained, the average γ' size and vol.% for each heat treatment, including the as-received condition, are showed in Table 4.4.

Table 4.4: γ' analysis summary

Heat treatment	γ' size [nm]	γ' vol.%
As-received (Solutionized)	43.84	21.57
Haynes standard	24.46	22.79
GKN standard	14.48 & 105.10	21.13
HT1	23.36	23.55
HT10	69.36	20.97
HT11	66.76	17.14
HT12	68.40	23.77

4.4.3 EDS

One of the objectives of the SEM analysis was the identification and classification of secondary carbides in the microstructure. This was carried out with an energy dispersive X-ray spectroscopy (EDS) analysis. This study was performed in selected areas, and the results obtained, Fig. 4.17, show the element distribution in the analyzed region. Based in the concentration observed, a confirmation of Cr-rich $M_{23}C_6$ and Mo-rich M_6C carbides was possible.

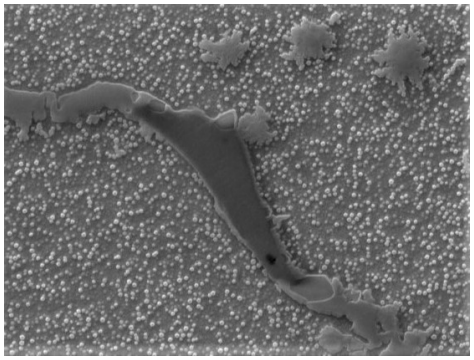

(a) Secondary carbides

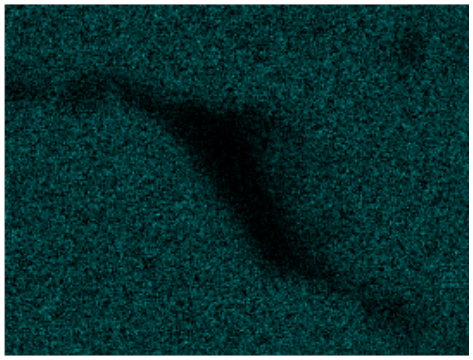

(b) Ni

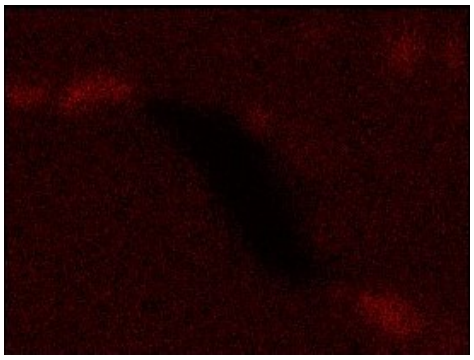

(c) Cr

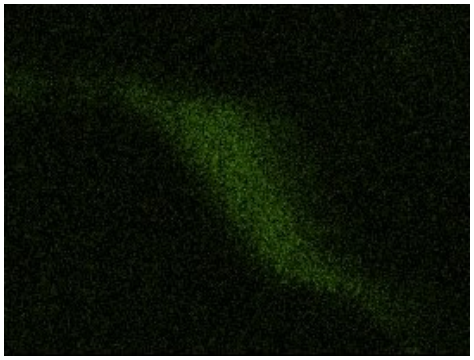

(d) Mo

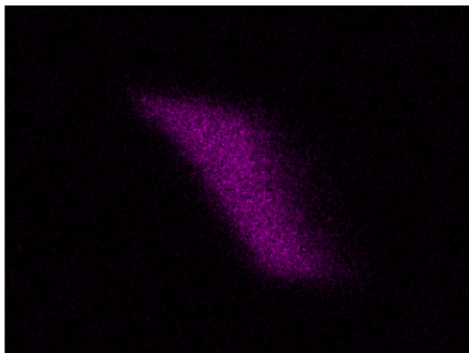

(c) Ti

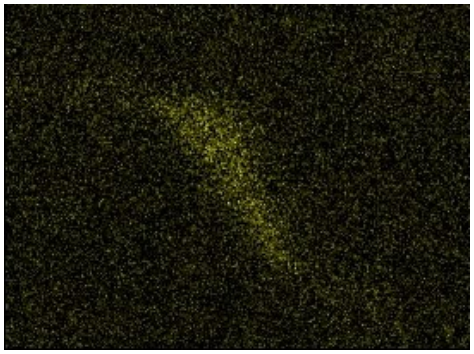

(d) C

Figure 4.17: EDS carbide identification

4.5 Tensile test

The results obtained from the tensile tests are presented in this section, for room temperature (RT) and elevated temperature at 750 °C.

In Fig. 4.18, the yield strength for each sample is plotted for both temperatures. It is possible to see that the highest performance at RT was observed in the GKN standard heat treatment, closely followed by Haynes standard and HT1. The lowest values were in HT10, HT11, and HT12 samples. At 750 °C, the difference in yield strength between the samples decreased, but GKN heat treatment remained the highest in average, while the rest of the heat treated samples show similar performance between them.

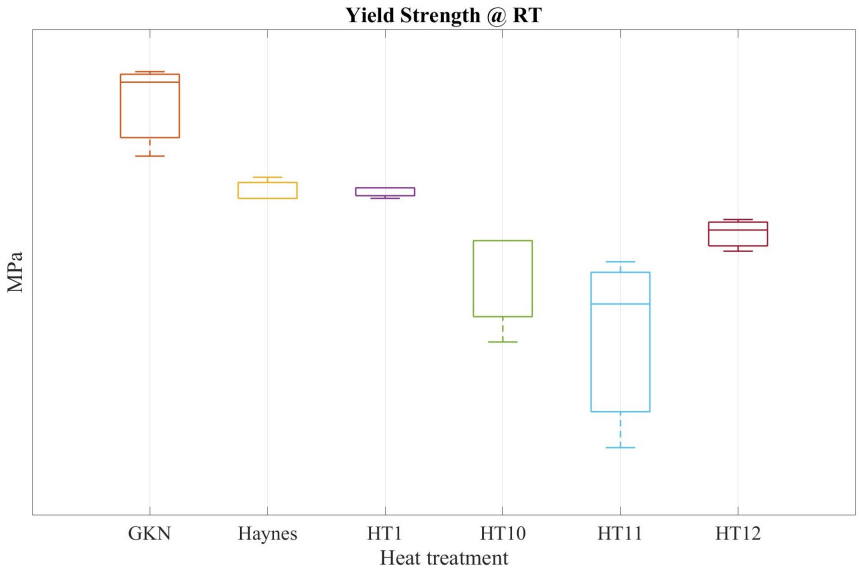

(a) Room Temperature

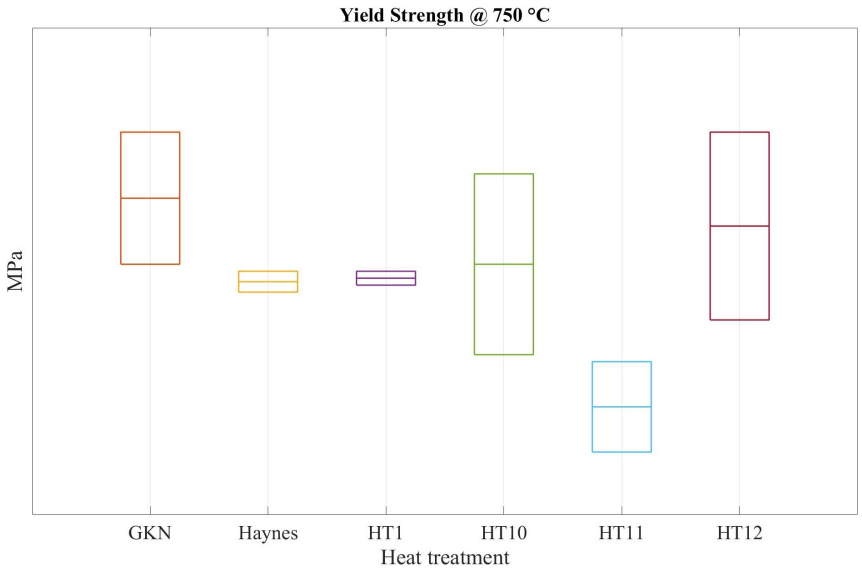

(b) 750°C

Figure 4.18: Tensile test results - Yield strength

Regarding the tensile strength of the samples, the results obtained can be observed in Fig. 4.19. At room temperature, GKN standard heat treatment sample still shows the highest average value, but when temperature was increased, the performance shifted. At 750 °C, HT12 showed the highest value, followed by HT10, Haynes standard and HT11; the lowest UTS at elevated temperature was found in the GKN standard sample.

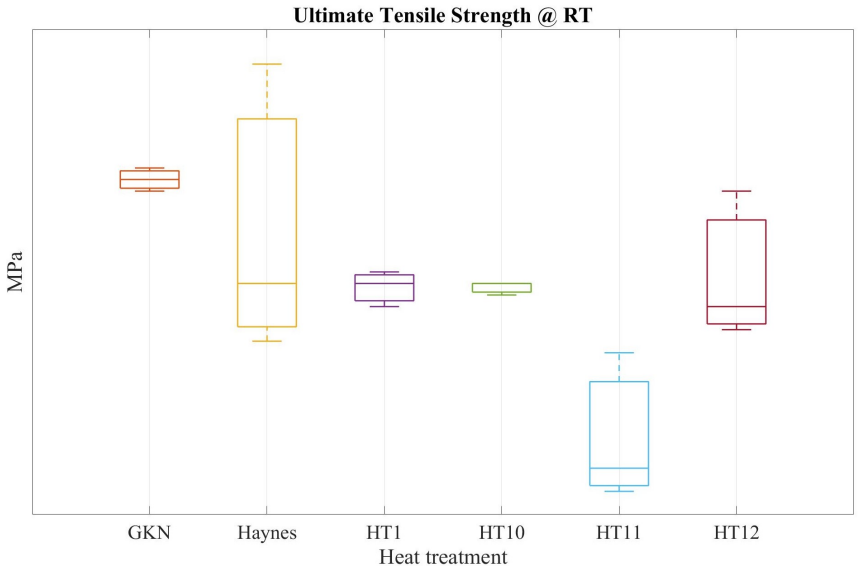

(a) Room Temperature

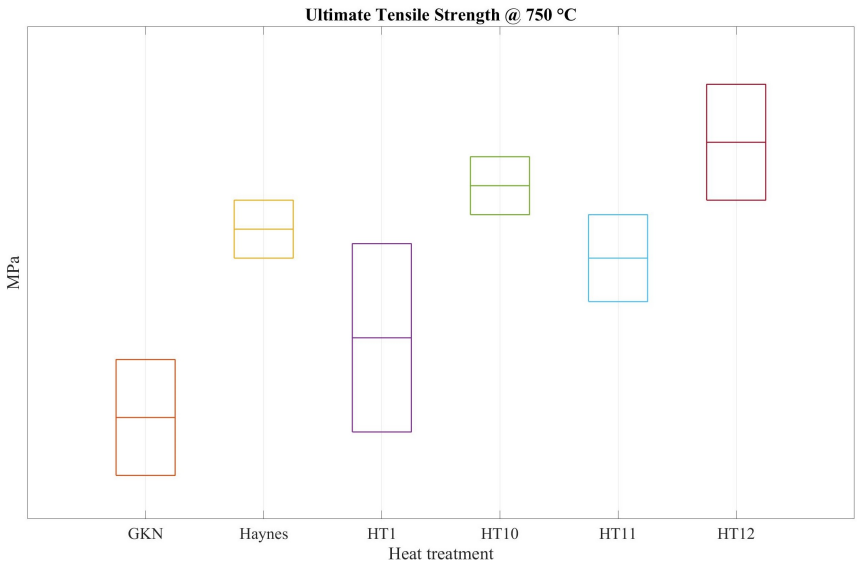

(b) 750°C

Figure 4.19: Tensile test results - Ultimate tensile strength

For ductility performance at room temperature, Fig. 4.20a, a higher elongation was observed in HT10, closely followed by Haynes standard heat treatment, and by HT12. At elevated temperatures, Fig. 4.20b, the increase in elongation was clearly seen in HT10 sample, now followed by Haynes standard, HT11 and HT12, while GKN standard heat treatment showed the lowest average value. Area reduction properties were also obtained, and the graphs can be observed in the Appendix of this report.

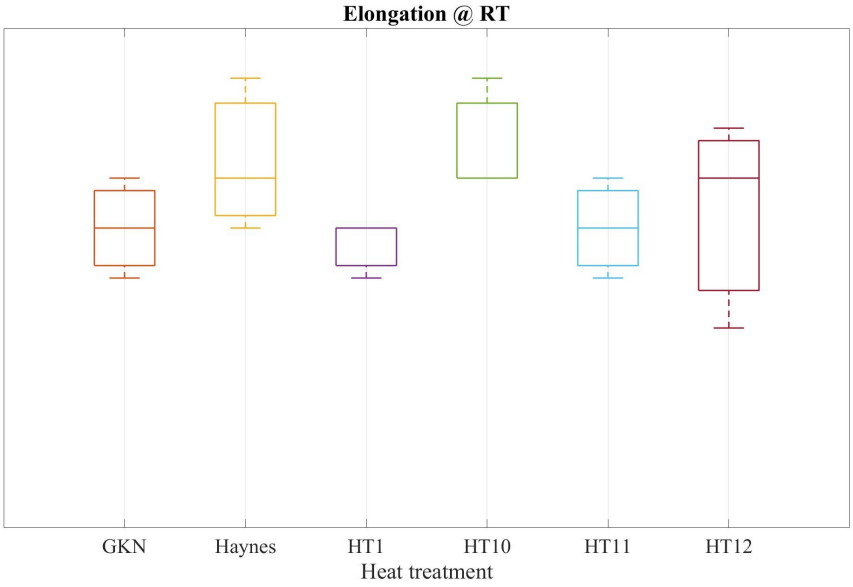

(a) Room Temperature

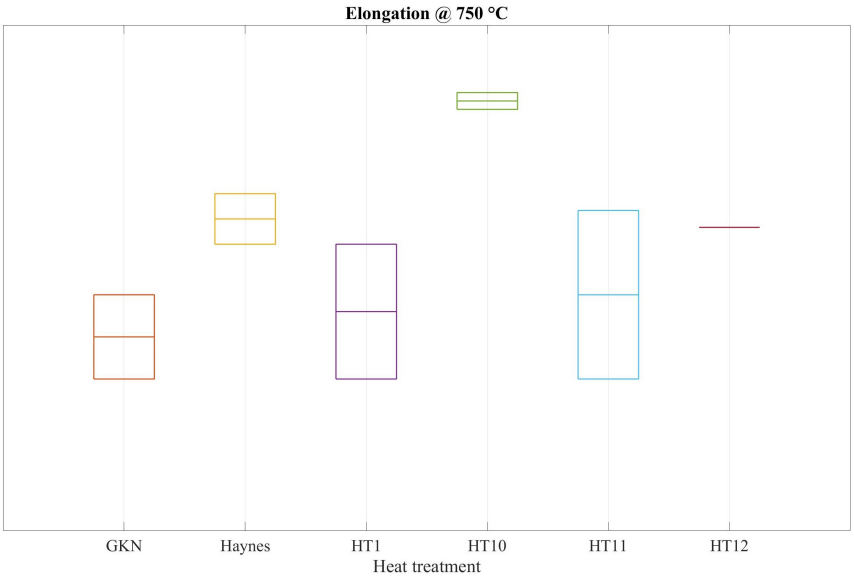

(b) 750°C

Figure 4.20: Tensile test results - Elongation

In Table 4.5 it is possible to see a summary of the values obtained from the tensile test at room temperature. In it, Haynes standard heat treatment values were taken as a reference point, while the rest show the difference in percentage against them, for each mechanical property. At room temperature, GKN standard sample shows the highest values in yield strength and tensile strength, while HT10 sample show the highest elongation and area reduction.

Table 4.5: Tensile test results at room temperature

Heat treatment	Yield strength	UTS	Elongation	Area reduction
Haynes standard	Ref.	Ref.	Ref.	Ref.
GKN standard	+ 7.5%	+ 3.0%	- 17.8%	+ 0.0%
HT1	+ 0.0%	- 3.5%	- 22.3%	- 19.1%
HT10	- 7.1%	- 3.5%	+ 5.5%	+ 20.3%
HT11	- 12.5%	- 12.6%	- 17.8%	- 10.9%
HT12	- 3.6%	- 2.8%	- 13.3%	- 17.2%

Table 4.6 presents the values for the tensile test at 750 °C, in which Haynes standard values were taken as reference points for comparison against the rest. At this temperature, GKN standard shows the highest yield strength, but for tensile strength is now HT12, while HT10 remains the highest in elongation and area reduction.

Table 4.6: Tensile test results at 750 °C

Heat treatment	Yield strength	UTS	Elongation	Area reduction
Haynes standard	Ref.	Ref.	Ref.	Ref.
GKN standard	+ 2.5%	- 8.7%	- 37.8%	- 21.1%
HT1	+ 0.1%	- 5.0%	- 29.7%	+ 34.2%
HT10	+ 0.5%	+ 2.0%	+ 37.8%	+ 34.2%
HT11	- 3.7%	- 1.3%	- 24.3%	- 18.4%
HT12	+ 1.7%	+ 4.0%	- 2.7%	+ 15.8%

The values obtained in the tensile tests saw an increase in most of the cases between room temperature and elevated temperature conditions. In order to analyze the change, the variation for each heat treatment can be observed in Table 4.7.

Table 4.7: Mechanical properties variation between RT and 750 °C

Heat treatment	YS variation	UTS variation	EL variation	AR variation
Haynes standard	- 12.6 %	+ 5.1 %	+ 153.4 %	+ 78.1 %
GKN standard	- 16.7 %	- 6.8 %	+ 91.7 %	+ 40.6 %
HT1	- 12.5 %	+ 3.5 %	+ 129.3 %	+ 195.4 %
HT10	- 5.4 %	+ 11.1 %	+ 231.2 %	+ 98.7 %
HT11	- 3.8 %	+ 18.7 %	+ 133.3 %	+ 63.2 %
HT12	- 7.8 %	+ 12.5 %	+ 184.4 %	+ 149.1 %

4.5.1 Containment factor

As mentioned previously, a direct way to measure the improvement of the mechanical properties after heat treatment is through the containment factor. This is measured with the formula $CF = 1/2 * (YS + UTS) * (Elongation)$. This parameter was calculated with the data obtained from the tensile test for both room and elevated temperatures, obtaining the graphs presented in Fig. 4.21.

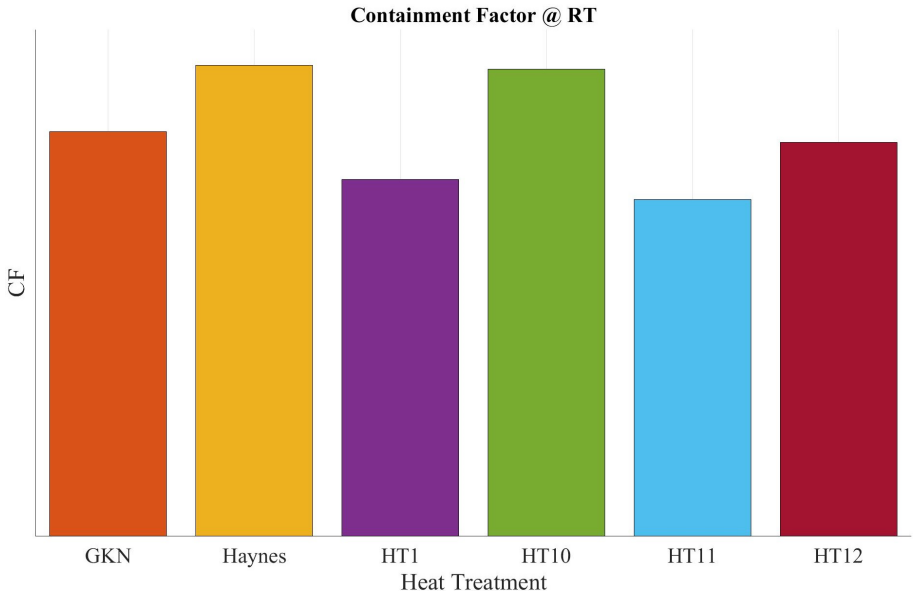

(a) Room Temperature

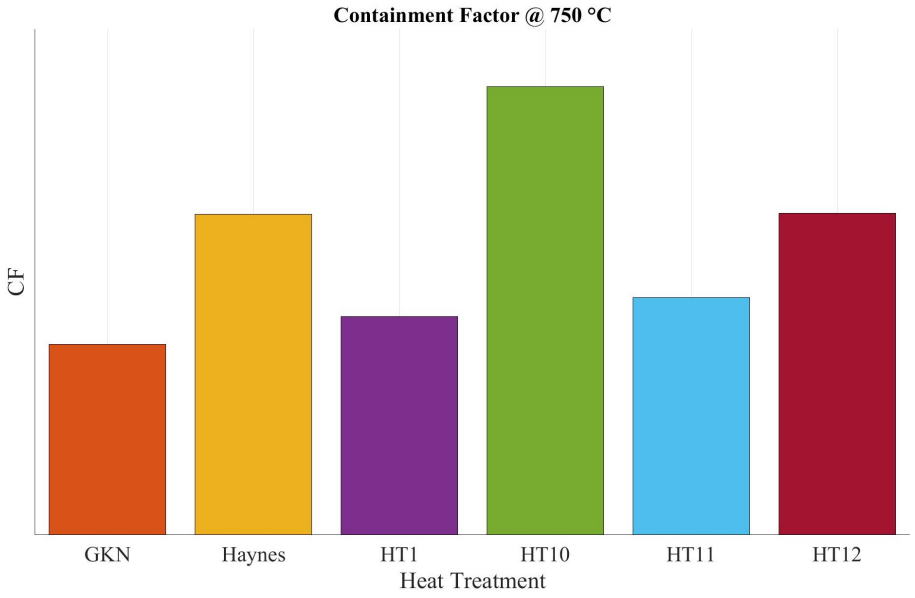

(b) 750 °C

Figure 4.21: Containment factor analysis

Based in the previous results, the change in percentage between temperatures for the containment factor of each heat treatment can be observed in Table 4.8.

Table 4.8: Containment factor variation between RT and 750 °C

Heat treatment	CF variation
Haynes standard	+ 246 %
GKN standard	+ 170 %
HT1	+ 221 %
HT10	+ 346 %
HT11	+ 254 %
HT12	+ 295 %

4.6 Carbide stabilization study

The carbide stabilization step analysis consisted in different tests, including hardness measurement, optical microscopy, and SEM analysis.

The hardness properties of the samples were obtained as described in section 3.3, resulting in the values shown in Table 4.9, where the Vickers hardness of the sample center region is represented. In this table, the 1065 °C treatment is represented with the T1 label, 1010 °C treatment with T2, and finally the 900 °C treatment with T3.

Table 4.9: Hardness - Carbide stabilization step analysis

Carbide stabilization step	Hardness [HV]
T1	181
T2	195
T3	241

Similar to the previous sections, a comparison was made between the surface and the center of the cast. The hardness measured in this comparison can be observed in Fig. 4.22. The same labels as the previous table were used.

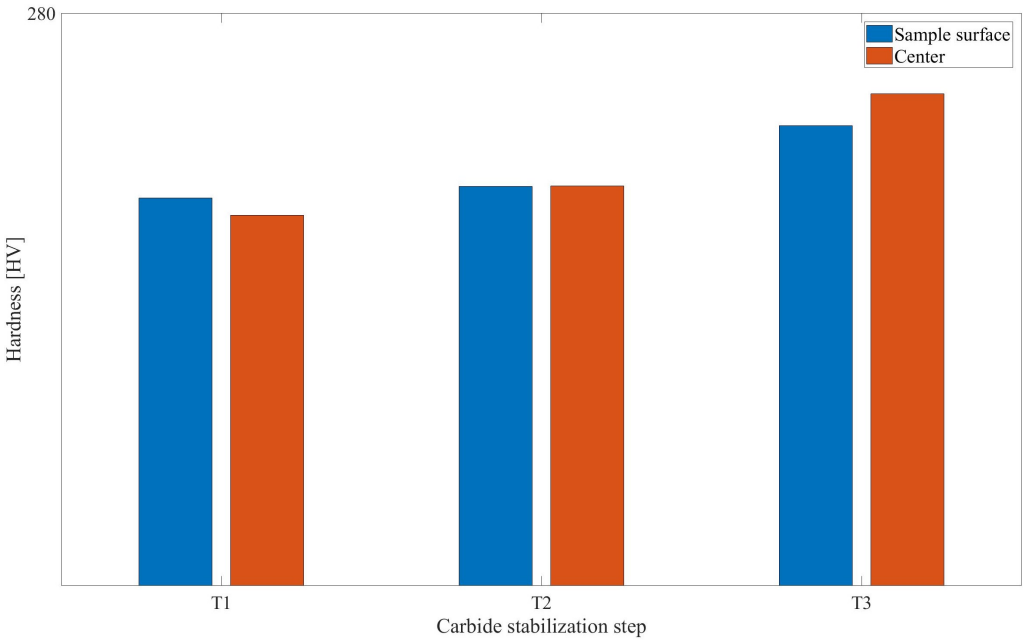

Figure 4.22: Hardness comparison - Carbide stabilization step analysis

The SEM analysis showed the different characteristics the microstructure presented during the different carbide stabilization processes. These characteristics can be observed in Fig. 4.23 for each carbide stabilization treatment. The analysis focused in the grain boundary carbides morphology.

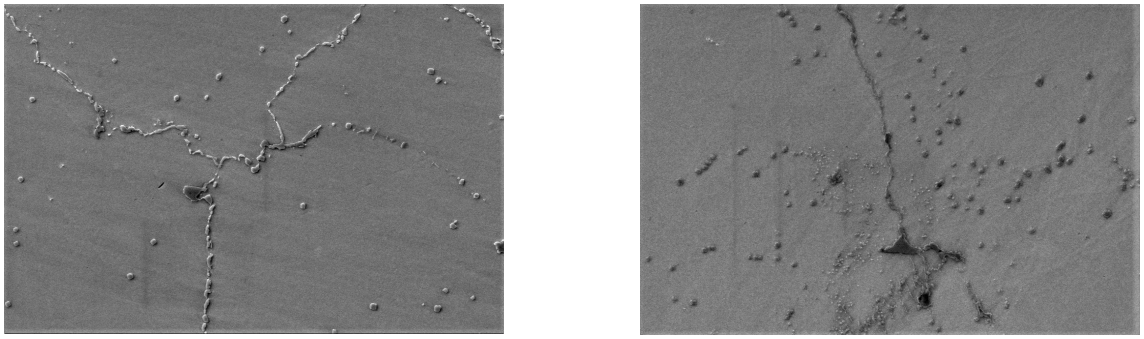

(a) 1065 °C / 2 hrs

(b) 1010 °C / 2 hrs

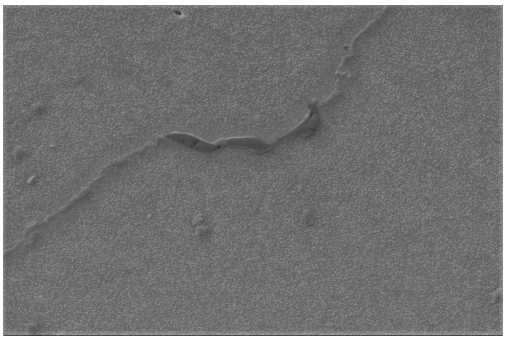

(c) 900 °C / 2 hrs

Figure 4.23: SEM of carbide stabilization step study

The final analysis of this additional study consisted in analyzing the characteristics of γ' found in the CS3 sample (900 °C / 2 hrs). From images obtained with SEM at high magnification, a distribution of the γ' size was obtained. In Fig. 4.24 it is possible to see the precipitation obtained from this carbide stabilization step, while on Fig. 4.25, the size distribution is shown, obtaining an average size of 47.39 nm.

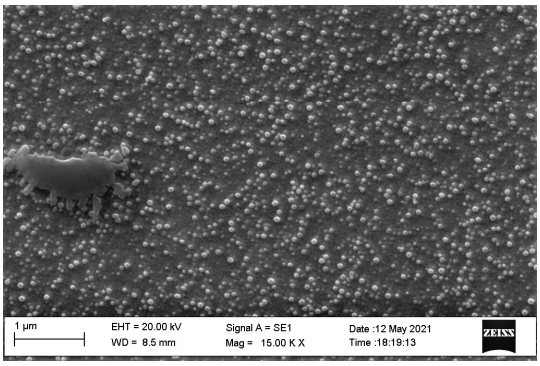

Figure 4.24: CS3 - γ' at high magnification

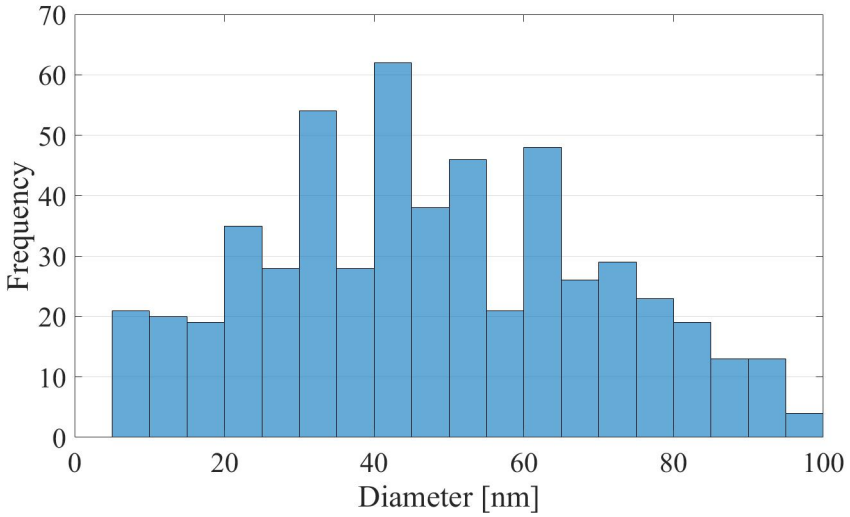

Figure 4.25: CS3 - γ' size distribution

5

Discussion

After all the information presented in section 4 was gathered, it was possible to compare the different results obtained. This sections explains in detail such comparison, in which the different properties observed are related to the heat treatments and their performance.

5.1 Tensile test - Heat treatment relation

One of the main relations that could be obtained from the tensile test and each heat treatment that was tested was the influence of γ' in the mechanical performance. There is evidence to state a relationship between the size and volume fraction of γ', with the yield strength (YS), tensile strength (UTS), and ductility properties of the material.

From the tensile test results, there were interesting changes in the material reflected in the different properties that were tested. For the yield strength results, there is a clear difference between the values obtained from the Haynes standard, GKN standard, and HT1 heat treatment, in comparison to the ones observed in HT10, HT11, and HT12, at room temperature. When comparing these values to the microstructure analysis results, it is possible to see a similar pattern in the samples when analyzing the γ' size they present. For the first three heat treatments, they all show an average size around 20 nm, while the latter three heat treatment alternatives show a bigger average size of approximately 68 nm. This points out to a direct effect from γ' size, in which a growth of 40 nm, approximately, is reflected in a decrease of the yield strength of 10 % in average. By analyzing each heat treatment individually, it was also concluded that a decrease in volume fraction of γ' also results in a decrease in yield strength. In HT11, it presented 17 vol.% of γ', and an 8% decrease in strength when compared to HT10 and HT12, which had similar γ' size and a higher fraction of 20.97 vol.% and 23.77 vol.%, respectively.

Similar to yield strength, the tensile strength observed follows the same pattern at room temperature, with the same implications of γ' size and fraction, and the effect they had in the tensile test results. There, the effect of lower volume fraction of γ' is seen more clearly for HT11. Additionally, now is possible to see a tendency of different strength values between HT10 and HT12, which parameters are the same except the application of step 0 in the latter one. The difference observed follows the expected performance observed in Haynes International patent, where the addition of that step resulted in an increase of strength, when compared to the same treatment without it.

Regarding the elongation values observed at room temperature, the effect of γ' size between the heat treatments is not fully reflected in the results, since the elongation

difference between the highest and the lowest values observed is only of 2%. It is important to note that the highest elongation in average is inclined towards HT10, HT11, HT12, which all present a bigger γ' in their microstructure, including the highest elongation that corresponds to HT10.

For the tensile tests results observed at high temperature, there are also important relationships that can be mentioned between the heat treatments. When the temperature was increased, in general there was an improvement of ductility, tensile strength, and containment properties for the proposed alternative heat treatments, and also in Haynes standard heat treatment.

For yield strength, GKN standard heat treatment remained the highest, but presented the largest decrease between room temperature and 750 °C, which can be expected due to its high initial value. It is also important to note that all the heat treatments presented average yield strength values not far from each other, with only 30 MPa between the highest value from GKN standard, and the lowest value from HT11. Similar to their performance at room temperature, Haynes standard and HT1 showed almost the same results between them, which is explained due to their similar heat treatment parameters, with a modified carbide stabilization step.

Inversely from the results observed at room temperature, the tensile strength values that were present at high temperature stated a similar difference, but now HT10, HT11 and HT12 were at the top, with HT12 being the highest. These last three heat treatments showed the largest strength increase between RT and 750 °C, in which HT11 increased the most, with 18.7% stronger than its performance at room temperature. Also, GKN standard heat treatment was the only one to decreased between room temperature and elevated, with a decrease of 6.8 %. One last important note in this aspect is the good performance of Haynes standard heat treatment, which did not increased much compared to its RT values, but still managed to have the third highest tensile strength.

The elongation observed at high temperature is the mechanical property with the highest difference from the tensile test performed. At 750 °C, the highest value, from HT10, presented more than twice the elongation of the lowest value, from GKN standard heat treatment. Another good performance was observed in Haynes standard and HT12 heat treatments, in which both increased more than 150 % from their initial RT value. By comparing the results observed at this temperature with the RT results, it is possible to say that the highest improvement between the temperatures are found in the heat treatment alternatives that showed the biggest γ' size at room temperature.

The relation of the mechanical properties observed at elevated temperature and the characteristics of γ' for each heat treatment could not by further studied due to limits in time. Due to this, an important next step is to analyze and understand the microstructure changes that occurred during the test, and how they relate to the mechanical properties improvements that were described.

5.2 Heat treatment parameters effects

Based in the observations described in the previous section, it was possible to determine the effects in the microstructure and mechanical performance, caused by the modifications done in each heat treatment.

Since the solution treatment step was not modified for any heat treatment, this step did not play a significant role in a specific heat treatment, and served as a common initial step for all the tested treatments. Despite there was no changes in this step, an important remark is that there was evidence of γ' precipitation already since this step. The consequences this may have is a variation in the final γ' size and volume fraction, depending on the target characteristics that are desired and the parameters used in the steps that followed.

The changes in time and temperature performed in the carbide stabilization step demonstrated the possibility to tailor the strength and ductility of the alloy. When the step temperature decreased from the recommended temperature of 1010 °C, it was possible to see an increase of ductility, as seen in HT10, HT11 and HT12, which was reflected in the containment factor afterwards. An important fact to consider is the precipitation step that follows it, since its parameters will also affect the precipitation of secondary phases. The analysis of HT10 and HT11, which had the same carbide stabilization step but different precipitation temperatures, showed that even if the carbide stabilization step is common, a different precipitation step can result in lower precipitation of γ', with the respective effect in the mechanical properties. Also, the decrease in carbide stabilization temperature is the most probable cause for an increase in γ', causing it to precipitate at this step, since it is below the solvus limit.

Regarding the time variation in the carbide stabilization step, it was possible to see two cases, depending if its temperature was above or below γ' solvus limit. As seen in the HT1 and Haynes comparison, if the temperature was above γ' limit, 997 °C according to literature, the increase in time did not affect significantly its precipitation, which was defined by the precipitation step that followed it. On the other hand, if the temperature was below it, a longer carbide stabilization step will be reflected in the growth of γ', with longer times resulting in a higher γ' size after the heat treatment.

For the precipitation step parameters, the relationship the temperature and time parameters had with γ' size and volume fraction was observed. As mentioned before, the previous steps of the heat treatment affected the microstructure obtained from the precipitation step, but it was possible to get an idea of the effects it had in the material. As seen in the simulations and in the SEM, an increase of temperature during precipitation results in lower volume fraction, while the size of γ' did not change much. This points out that the main effect temperature has in this step is reflected in a variation in strength, due to lower precipitation frequency of γ', based in the tensile tests results and γ' distribution. The variation of time in this step was not studied, and it was not possible to relate experimentally its variation with any specific change.

The additional optional step, called Step 0, before the carbide stabilization step was studied in HT12 and compared directly with HT10, which presented the same heat treatment without the additional step. From the results obtained, it was confirmed that ductility is improved, but not as much as the heat treatment without the Step 0. HT10 presented higher ductility than Haynes and GKN standard heat treatments at both RT and elevated temperature, while HT12 only was higher at elevated temperatures. This is later balanced with less decrease in yield and tensile strength, in which both showed lower yield and tensile strength than the reference heat treatments at room temperature, but at elevated temperature, HT12 presented the highest tensile strength.

In general. the parameters variation in these two steps, carbide stabilization and precipitation, confirms the possibility to increase ductility, specially at high temperatures, with an expected decrease in strength. Based in the results observed in this thesis, it is possible to arrive to an ideal combination of heat treatment parameters that results in improved ductility and minimize the decrease in strength, with an adequate γ' size and volume fraction.

5.2.1 Containment factor improvement

When the results obtained were translated into containment factor terms, it was possible to see a relevant increase in some heat treatments, confirming the potential they have for improving mechanical properties, specially at elevated temperatures.

A good way to summarize and compare the performance of each heat treatment, as mentioned before, is with the containment factor described in the previous sections. Firstly, it was possible to see the high importance ductility properties have in the containment properties measurement. This was observed with the Haynes standard and HT10 heat treatments at room temperature, in which both did not present the highest value for yield nor tensile strength, but balanced it with medium strength values and good elongation results. Related to this, the low elongation values presented by GKN standard heat treatment directly affected its CF value, locating it in a middle position, when compared to the other heat treatments.

At high temperature, these differences were stated more clearly, due to the fact that UTS and elongation values showed a significant increase for certain heat treatments. As mentioned in the previous section, the difference between the highest elongation of HT10 and the lowest of GKN standard heat treatment was significant. This was reflected in the CF values, where HT10 containment factor was 235% more than what GKN presented. It is also important to note that the difference in yield strength also decreased between the heat treatments, which also contributed to this change. Another important phenomena observed at elevated temperature is the good performance of both Haynes standard and HT12 heat treatment, which improvements were also reflected in the containment factor, almost twice the value of GKN standard heat treatment.

In order to confirm the containment properties improvement at elevated temperatures, it is possible to perform more specialized test. These tests can vary in their methods, for example they can use a special specimen geometry or a modified strain rate condition, but have a common objective to obtain more refined stress data. This information can eventually be used in simulation models for a specific component. Still, the formula that was used for this thesis is an accepted method to measure containment properties in the industry, reaffirming the importance of material's ductility.

5.3 Carbide stabilization study analysis

Based on the hardness values measured and the images observed through SEM, it is possible to state the main changes cast Haynes 282 microstructure goes through after the carbide stabilization step of the heat treatment.

From the hardness tests, an increase in hardness was recorded when a lower temperature was applied. A difference of 33 % was observed between the highest temperature tested, 1065°C, and the lowest temperature, 900 °C. The increase in hardness is explained with the SEM analysis at high magnification, where γ' could be observed in this sample, and not in the others. When considering the average size of 47.39 nm from the observed γ' , it can be concluded that the samples treated at this temperature have started the precipitation and growth of γ' since this step, and a further precipitation step will contribute in their growth.

In addition to this, the increase of hardness in the center region showed up during this step only in the lowest temperature treatment. The fact that the hardness difference is only observed in those conditions increases the possibility that it is caused because of the solute segregation within the sample, resulting in a distribution difference of γ' during its precipitation. The reason of this is that the other two samples treated at higher temperatures went through similar cooling rates and did not showed a difference in hardness between the surface and the center region, highlighting the lack of γ' in them.

Finally, it was possible to see some secondary carbides in the sample treated at 1065°C but with lower frequency, compared to the samples treated at lower temperatures. Related to this, the microstructure observed at the highest temperature presented blocky discrete grain boundary carbides and, as the temperature decreased, they adopted a more continuous morphology until a continuous film was reached at 900 °C.

6

Conclusion

In this thesis several heat treatment alternatives for cast Haynes 282 were proposed, tested and evaluated with the purpose of improving its mechanical properties at room and elevated temperature. Based in the results and analysis obtained in this work, the following conclusions can be made:

- Simulation tools were a good initial approach for heat treatment design, although final values deviated with results obtained experimentally.
- The casting conditions before heat treatment have effect on the results obtained, as seen in the hardness and γ' characteristics observed.
- The heat treatments proposed that showed potential in improving ductility and containment properties at room temperature is HT10, compared to GKN and Haynes standard.
- At elevated temperature, the heat treatments alternative that presented improvement in ductility, tensile strength and containment properties are HT10 and HT12, in comparison to GKN and Haynes standard heat treatments.
- Haynes standard heat treatment showed an acceptable performance considering strength, ductility and containment at both temperatures, in comparison with GKN standard and alternative heat treatments.
- The relation of γ' size and distribution with tensile test results was confirmed, in which bigger size and/or lower fraction resulted in lower yield and tensile strength at room temperature.
- A higher γ' size after heat treatment resulted in an increase in elongation, specially at elevated temperatures.
- The importance of mechanical and containment properties at elevated temperature in aerospace applications supports further studies in the proposed heat treatments H10 and HT12.
- Specialized containment tests can be performed to confirm the improvement in HT10 and HT12, with a specific component requirements approach.
- Further studies on untested heat treatments alternatives mentioned in this thesis are encouraged, to continue the analysis of the relation between mechanical properties and microstructural changes due to heat treatment.

Bibliography

[1] M. J. Donachie and S. J. Donachie, *Superalloys: A Technical Guide. ASM International, 2008.* The Materials Information Society, 2002.

[2] P. D. Jablonski, J. A. Hawk, C. J. Cowen, and P. J. Maziasz, "Processing of advanced cast alloys for A-USC steam turbine applications," *JOM*, vol. 64, 2012.

[3] Haynes International, "Haynes® 282® alloy," 2020. Haynes 282 Brochure H-3173D.

[4] J. A. Hawk, T. L. Cheng, J. S. Sears, P. D. Jablonski, and Y. H. Wen, "Gamma prime stability in Haynes 282: Theoretical and experimental considerations," *Journal of Materials Engineering and Performance*, vol. 24, 2015.

[5] C. Joseph, *Microstructure evolution and mechanical properties of haynes 282.* PhD thesis, Chalmers University of Technology, 2018.

[6] A. D. Gianfrancesco, "15.1.1.1 composition of Haynes 282 alloy in comparison to other wrought gamma alloys," *Materials for Ultra-Supercritical and Advanced Ultra-Supercritical Power Plants*, 2017.

[7] A. Polkowska, W. Polkowski, M. Warmuzek, N. Cieśla, G. Włoch, D. Zasada, and R. M. Purgert, "Microstructure and hardness evolution in haynes 282 nickel-based superalloy during multi-variant aging heat treatment," *Journal of Materials Engineering and Performance*, vol. 28, 2019.

[8] P. D. Jablonski and J. A. Hawk, "Homogenizing advanced alloys: Thermodynamic and kinetic simulations followed by experimental results," *Journal of Materials Engineering and Performance*, vol. 26, 2017.

[9] C. Joseph, C. Persson, and M. Hörnqvist Colliander, "Influence of heat treatment on the microstructure and tensile properties of ni-base superalloy haynes 282," *Materials Science and Engineering: A*, vol. 679, pp. 520–530, 2017.

[10] H. Matysiak, M. Zagorska, J. Andersson, A. Balkowiec, R. Cygan, M. Rasinski, M. Pisarek, M. Andrzejczuk, K. Kubiak, and K. J. Kurzydlowski, "Microstructure of haynes® 282® superalloy after vacuum induction melting and investment

casting of thin-walled components," *Materials*, vol. 6, 2013.

[11] Y.-J. Kim, J.-H. Park, and Y.-S. Ahn, "Comparison of creep properties of cast and wrought Haynes 282 superalloy," *Advances in Materials Science and Engineering*, vol. 2018, 2018.

[12] M. G. Fahrmann and L. M. Pike, "Experimental TTT diagram of Haynes 282 alloy," vol. 2018-June, 2018.

[13] Y. Yang, R. C. Thomson, R. M. Leese, and S. Roberts, "Microstructural evolution in cast haynes 282 for application in advanced power plants," 2014.

[14] K. Y. Shin, J. H. Kim, M. Terner, B. O. Kong, and H. U. Hong, "Effects of heat treatment on the microstructure evolution and the high-temperature tensile properties of haynes 282 superalloy," *Materials Science and Engineering A*, vol. 751, 2019.

[15] L. Pike, "Heat treatments for improved ductility of Ni-Cr-Co-Mo-Ti-Al Alloys," June 2019. International Publication Number WO 2019/125637 A2.

[16] O. Adegoke, "Homogenization of precipitation hardening nickel based superalloys," Master's thesis, Högskolan Dalarna, 2012.

[17] S. Haas, J. Andersson, M. Fisk, J. S. Park, and U. Lienert, "Correlation of precipitate evolution with vickers hardness in haynes® 282® superalloy: In-situ high-energy saxs/waxs investigation," *Materials Science and Engineering A*, vol. 711, 2018.

[18] F. Hanning, A. K. Khan, J. Steffenburg-Nordenström, O. Ojo, and J. Andersson, "Investigation of the effect of short exposure in the temperature range of 750–950°c on the ductility of haynes® 282® by advanced microstructural characterization," *Metals*, vol. 9, 2019.

[19] Sente Software Ltd., "JMat Pro, version 12.4.."

[20] J.O. Andersson, T. Helander, L. Höglund, P.F. Shi, and B. Sundman, "Thermo-Calc and DICTRA version 2020b, computational tools for materials science.," 2002. Calphad, 26, 273-312.

[21] Thermo-Calc Software 2020b, "TCS Ni-based superalloys database (TCNI10)," 2020.

[22] ASTM, "E407-07(2015)e1, Standard Practice for Microetching Metals and Alloys, ASTM International, West Conshohocken, PA, 2015," *American Society for Testing and Materials*, vol. 07, 2015.

[23] ASTM, "Astm e140-12b. Standard Hardness Conversion Tables for Metals Relationship Among Brinell Hardness, Vickers Hardness, Rockwell Hardness, Superficial Hardness, Knoop Hardness, Scleroscope Hardness, and Leeb Hardness,"

American Society for Testing and Materials, 2012.

A

Appendix

In this section it is possible to find complementary information, including graphs, tables and images, in relation to different aspects mentioned in the report.

A.1 JMat Pro complete γ' simulations

In the following tables, A.1 - A.6, it is possible to observe the complete set of simulations done to analyze the changes in size and volume fraction of γ' with different combinations of heat treatment parameters.

Table A.1: JMat Pro simulations for precipitation time variation - Constant carbide stabilization step

Carbide stabilization step	Precipitation step	γ' size [nm]	γ' volume fraction [%]]
1010 °C - 2 hours	788 °C - 2 hours	21.99	17
1010 °C - 2 hours	788 °C - 4 hours	24.08	17
1010 °C - 2 hours	788 °C - 8 hours	27.41	17
1010 °C - 2 hours	788 °C - 16 hours	32.18	17

Table A.2: JMat Pro simulations for precipitation temperature variation - Constant carbide stabilization step

Carbide stabilization step	Precipitation step	γ' size [nm]	γ' volume fraction [%]]
1010 °C - 2 hours	730 °C - 8 hours	21.92	19
1010 °C - 2 hours	760 °C - 8 hours	23.62	18
1010 °C - 2 hours	788 °C - 8 hours	27.41	17
1010 °C - 2 hours	850 °C - 8 hours	45.67	14

Table A.3: JMat Pro simulations for carbide stabilization temperature variation - Constant precipitation step (8 hours)

Carbide stabilization step	Precipitation step	γ' size [nm]	γ' volume fraction [%]]
850 °C - 2 hours	788 °C - 8 hours	35.93	17
900 °C - 2 hours	788 °C - 8 hours	55.17	17
930 °C - 2 hours	788 °C - 8 hours	78.09	17
950 °C - 2 hours	788 °C - 8 hours	102.17	17

Table A.4: JMat Pro simulations for carbide stabilization temperature variation - Constant precipitation step (4 hours)

Carbide stabilization step	Precipitation step	γ' size [nm]	γ' volume fraction [%]]
850 °C - 2 hours	788 °C - 4 hours	34.13	17
900 °C - 2 hours	788 °C - 4 hours	54.41	17
930 °C - 2 hours	788 °C - 4 hours	77.23	17
950 °C - 2 hours	788 °C - 4 hours	101.93	17

Table A.5: JMat Pro simulations for carbide stabilization and precipitation step with time and temperature variation

Carbide stabilization step	Precipitation step	γ' size [nm]	γ' volume fraction [%]]
900 °C - 4 hours	730 °C - 8 hours	69.81	19
900 °C - 4 hours	760 °C - 8 hours	69.18	18
900 °C - 4 hours	788 °C - 8 hours	68.07	17
900 °C - 4 hours	850 °C - 8 hours	70.12	14

Table A.6: JMat Pro simulations for carbide stabilization and precipitation step with time and temperature variation

Carbide stabilization step	Precipitation step	γ' size [nm]	γ' volume fraction [%]]
900 °C - 2 hours	730 °C - 8 hours	56.01	19
900 °C - 2 hours	760 °C - 8 hours	55.21	18
900 °C - 2 hours	788 °C - 8 hours	55.17	17
900 °C - 2 hours	850 °C - 8 hours	60.17	14

A.2 Hardness complementary graph

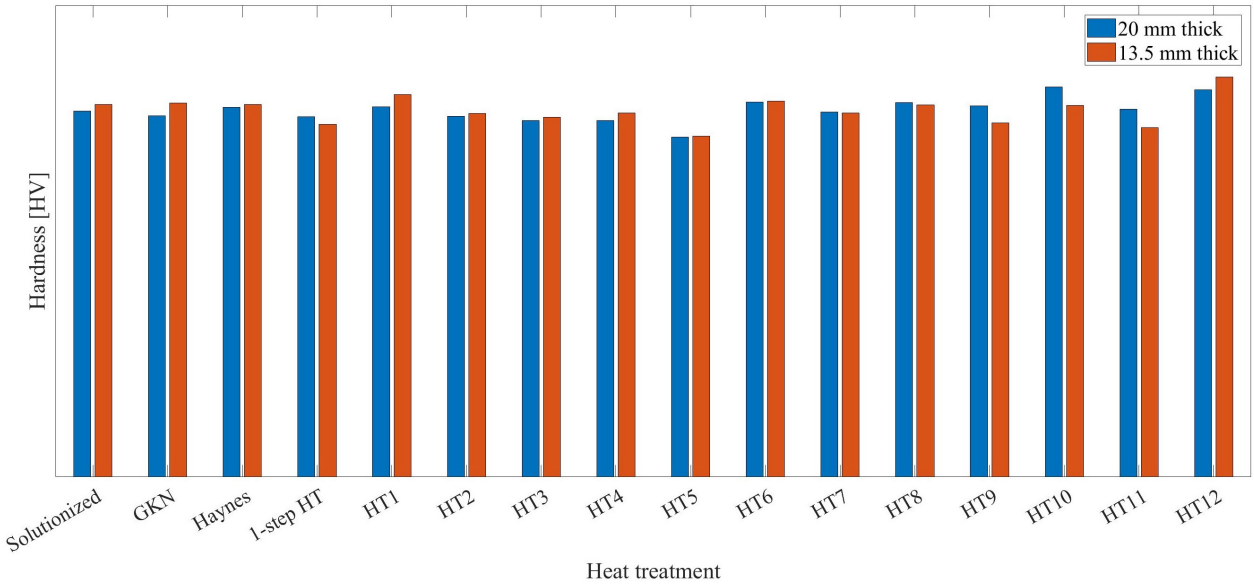

Figure A.1: Hardness comparison - Thick and thin cube samples at surface

A.3 Optical microscopy complementary images

The following images function as a complementary representation of aditional heat treatments, which were not used for tensile testing.

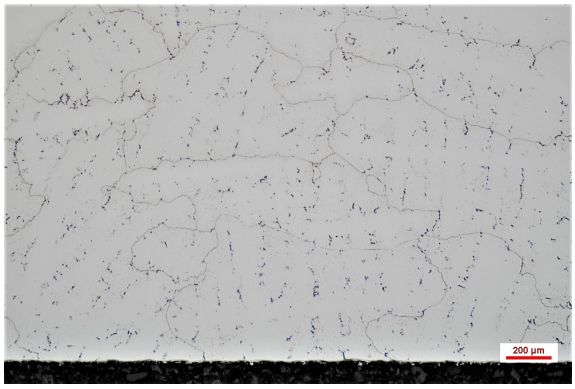

(a) As-received conditions - x50

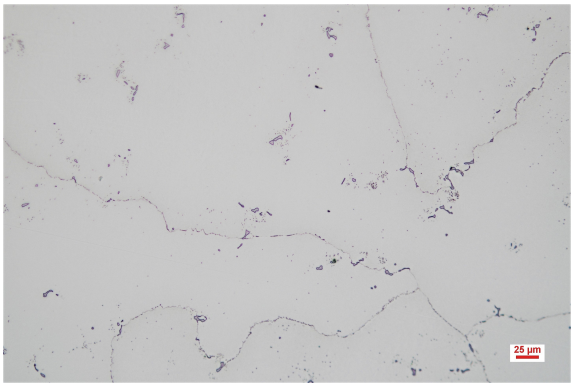

(b) As-received conditions - x200

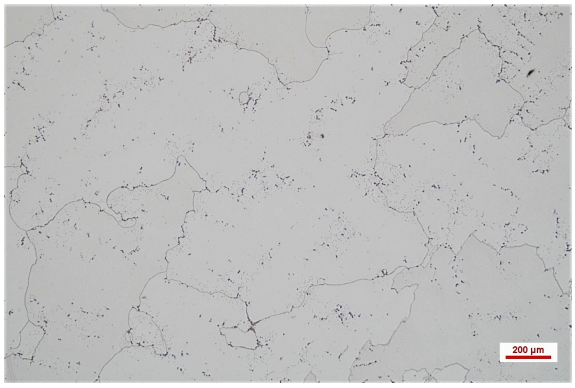

(c) HT5 - x50

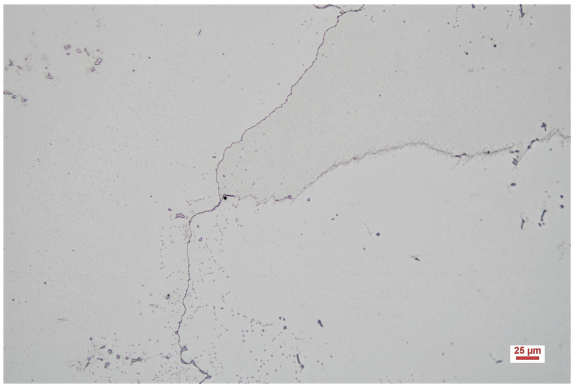

(d) HT5 - x200

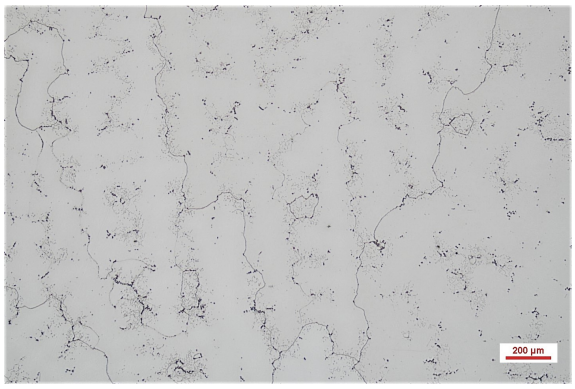

(c) HT6 - x50

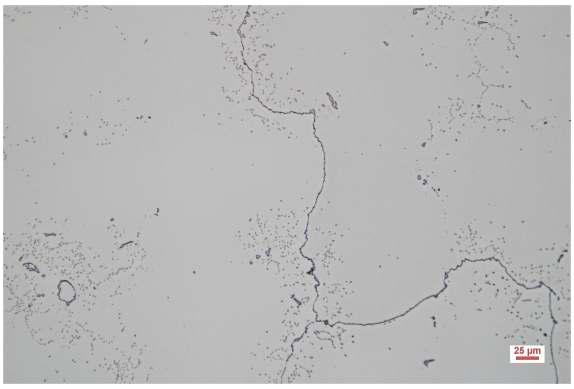

(d) HT6 - x200

Figure A.2: Additional optical microscopy for non-tensile tested samples

The following figure compares the different etchants used for optical microscopy, where the second etchant, oxalic acid, was the one selected for SEM analysis.

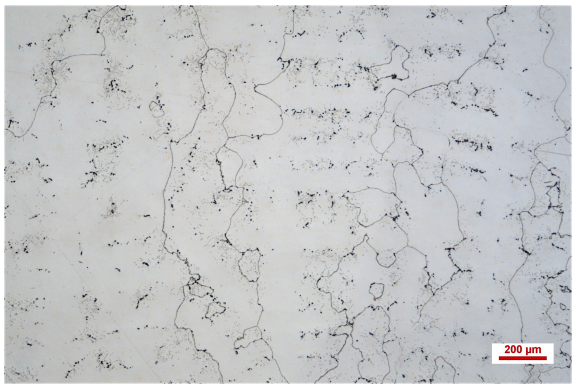

(a) GKN - x50 - HCl + H_2O_2 etching

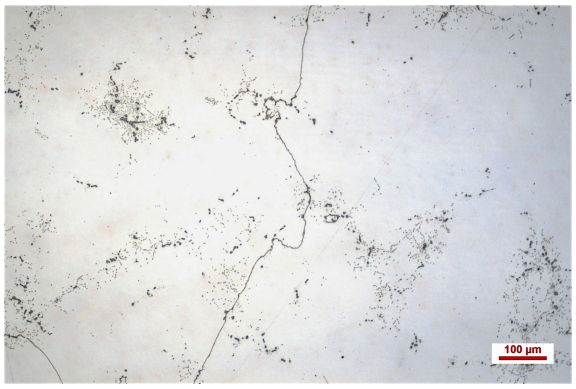

(b) GKN - x100 - HCl + H_2O_2 etching

(c) GKN - x50 - Oxalic acid etching

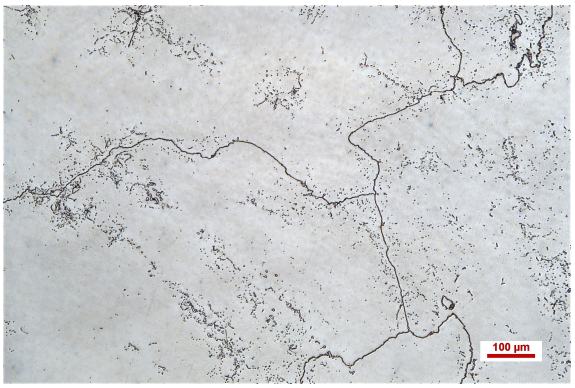

(d) GKN - x100 - Oxalic acid etching

Figure A.3: Etchants comparison for optical microscopy

In the following images, it is possible to observe the heat treated samples during the optical microscopy analysis using the oxalic acid etching.

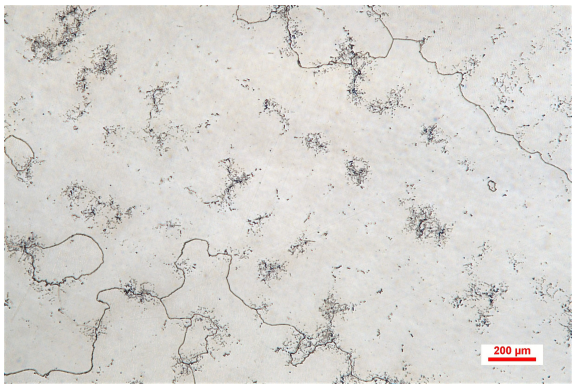

(a) Haynes standard HT - x50

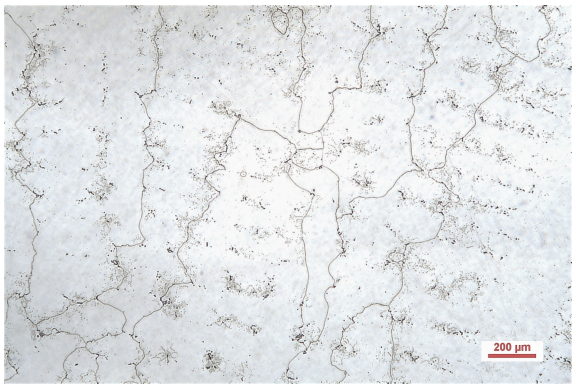

(b) GKN standard HT - x50

(c) HT1 - x50

(d) HT10 - x50

(c) HT11 - x50

(d) HT12 - x50

Figure A.4: Optical microscopy of oxalic acid etched samples

A.4 Tensile test complementary graphs

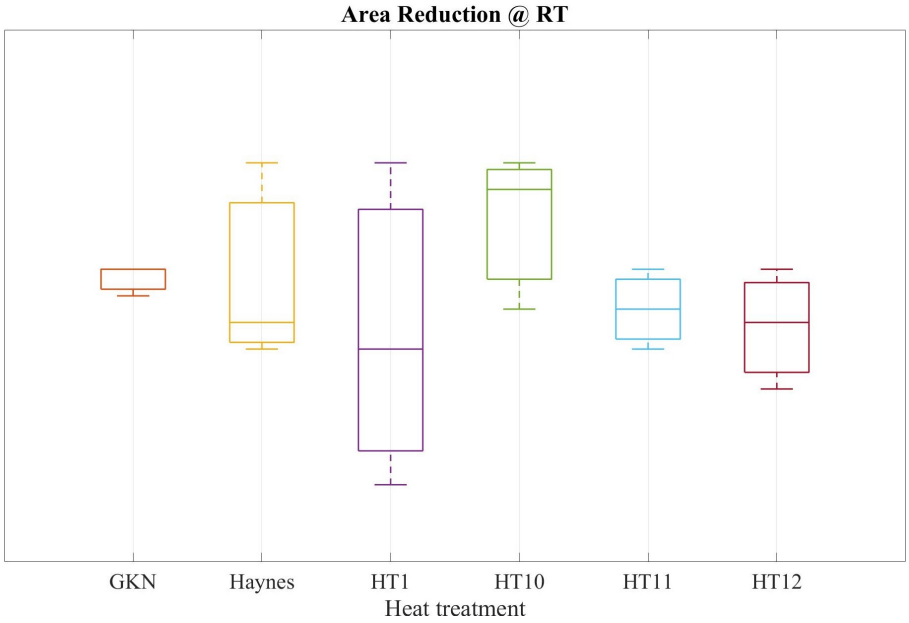

(a) Room Temperature

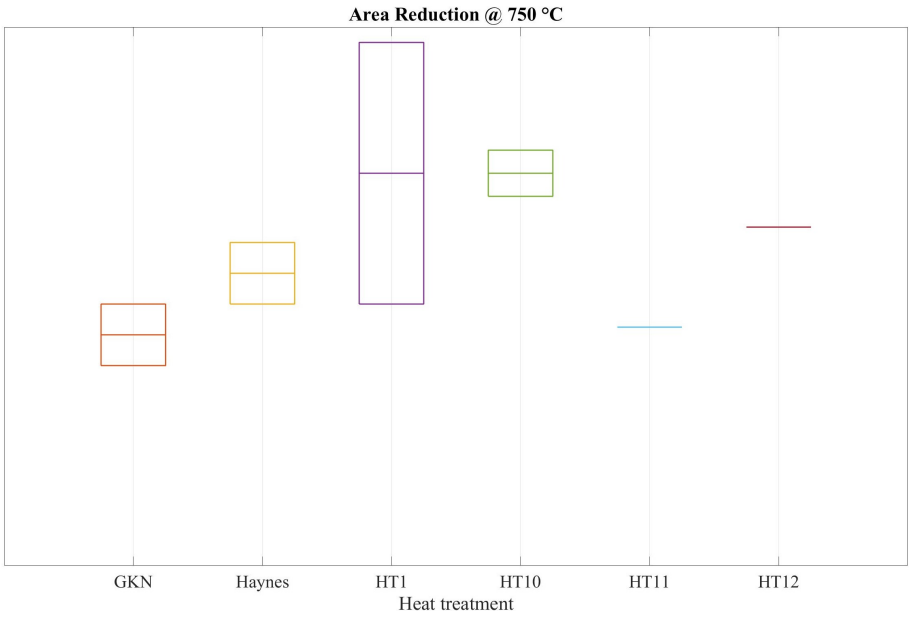

(b) 750°C

Figure A.5: Tensile test results - Area reduction

DEPARTMENT OF INDUSTRIAL AND MATERIALS SCIENCE
CHALMERS UNIVERSITY OF TECHNOLOGY
Gothenburg, Sweden
www.chalmers.se

CHALMERS
UNIVERSITY OF TECHNOLOGY